Exp Fluids (2011) 51:1261–1281
DOI 10.1007/s00348-011-1143-x

RESEARCH ARTICLE

Comparison of turbulent channel and pipe flows with varying Reynolds number

H. C. H. Ng · J. P. Monty · N. Hutchins · M. S. Chong · I. Marusic

Received: 28 May 2011 / Accepted: 8 June 2011 / Published online: 25 June 2011

Abstract Single normal hot-wire measurements of the streamwise component of velocity were taken in fully developed turbulent channel and pipe flows for matched friction Reynolds numbers ranging from $1{,}000 \leq Re_\tau \leq 3{,}000$. A total of 27 velocity profile measurements were taken with a systematic variation in the inner-scaled hot-wire sensor length l^+ and the hot-wire length-to-diameter ratio (l/d). It was observed that for constant $l^+ = 22$ and $l/d \gtrsim 200$, the near-wall peak in turbulence intensity rises with Reynolds number in both channels and pipes. This is in contrast to Hultmark et al. in J Fluid Mech 649:103–113, (2010), who report no growth in the near-wall peak turbulence intensity for pipe flow with $l^+ = 20$. Further, it was found that channel and pipe flows have very similar streamwise velocity statistics and energy spectra over this range of Reynolds numbers, with the only difference observed in the outer region of the mean velocity profile. Measurements where l^+ and l/d were systematically varied reveal that l^+ effects are akin to spatial filtering and that increasing sensor size will lead to attenuation of an increasingly large range of small scales. In contrast, when l/d was insufficient, the measured energy is attenuated over a very broad range of scales. These findings are in agreement with similar studies in boundary layer flows and highlight the need to carefully consider sensor and anemometry parameters when comparing flows across different geometries and when drawing conclusions regarding the Reynolds number dependency of measured turbulence statistics. With an emphasis on accuracy, measurement resolution and wall proximity, these measurements are taken at comparable Reynolds numbers to currently available DNS data sets of turbulent channel/pipe flows and are intended to serve as a database for comparison between physical and numerical experiments.

H. C. H. Ng · J. P. Monty · N. Hutchins · M. S. Chong · I. Marusic (✉)
Department Mechanical Engineering,
The University of Melbourne, Melbourne, VIC, Australia
e-mail: imarusic@unimelb.edu.au

H. C. H. Ng
e-mail: h.ng4@pgrad.unimelb.edu.au

1 Introduction

Of the three canonical wall bounded flows, channels and pipes differ from the flat plate zero pressure gradient boundary layer in that the outer length scale (the channel half-height h, or pipe radius R or boundary layer thickness δ) is fixed in channels and pipes, being confined by the opposing wall(s), whereas in a boundary layer, there is no such restriction and δ is free to grow. Henceforth, channel and pipe flows will be referred to as 'internal' flows and the boundary layer as an 'external' flow. For internal flows, the fixed outer length scale means that the viscous or inner length scale (ν/U_τ, where ν is the kinematic viscosity and U_τ the friction velocity) becomes increasingly small with increasing Reynolds number. However, as the friction Reynolds number represents the ratio of outer to inner length scales ($Re_\tau = \delta U_\tau/\nu$), it needs to be sufficiently high for there to be a separation of the small and large scales of turbulent motion, not to mention the formation of a logarithmic region of overlap between the inner and outer regions as put forward by classical scaling arguments. This poses a unique challenge for any experimental researcher of internal flows because for a fixed sensor size, be it the sensing element length of a hot-wire probe or the measurement volume used in LDV (Laser Doppler Velocimetry) and PIV (Particle Image Velocimetry) measurements,

increasing the Reynolds number will come at the expense of measurement resolution and wall proximity.

There have been many experimental studies of internal geometries that have contributed significantly to our current understanding of the physics of wall turbulence (for example, Laufer 1950, 1954; Comte-Bellot 1965; Morrison and Kronauer 1969; Lawn 1971; Perry and Abell 1975; Johansson and Alfredsson 1982, 1983; Wei and Willmarth 1989; Niederschulte et al. 1990; Eggels et al. 1994; Durst et al. 1995; den Toonder and Nieuwstadt 1997; Morrison et al. 2004; Monty 2005; Hultmark et al. 2010). However, there remain uncertainties in the database of velocity measurements available due to the wide range of influential measurement parameters and flow conditions. For example, the LDV studies listed above are at low Reynolds number not exceeding $Re_\tau \approx 1{,}700$. On the other hand, for all of the higher Reynolds number studies using hot-wires, the hot-wire sensor lengths were not controlled (with the exception of Hultmark et al. 2010), leading to varying spatial resolution effects as noted by Johansson and Alfredsson (1983). In addition, as pointed out by Monty (2005), the facilities of many studies with internal geometries have limited development length with the majority allowing for less than 100 channel heights H, or pipe diameters D, for flow development (with the exceptions of: den Toonder and Nieuwstadt 1997; Morrison et al. 2004; Hultmark et al. 2010). The Princeton 'Superpipe' data of Morrison et al. (2004) are unique in that the Reynolds numbers achieved in that study, $Re_\tau = \mathrm{O}(10^5)$, are two orders of magnitude higher than what is otherwise available for internal flows; however, there are documented spatial filtering issues and a limited wall proximity at those very high Reynolds numbers. These caveats should be carefully considered when examining the Reynolds number dependence of turbulence quantities measured in experiments, and recent work by Hutchins et al. (2009) suggests that particular emphasis should be placed on the measurement resolution and sensor/anemometer parameters.

Numerical simulations of internal flows have progressed remarkably during the last three decades. The first DNS of fully developed turbulent channel flow reported in Kim et al. (1987) was conducted at a friction Reynolds number of $Re_\tau = 190$, and current DNS data sets are available up to Reynolds numbers of $Re_\tau \approx 2{,}000$ in channel flows (Iwamoto et al. 2004, 2005; del Álamo et al. 2004; Hoyas and Jiménez 2006) and $Re_\tau \approx 1{,}100$ in pipe flows (Wu and Moin 2008). The accuracy of these simulations is limited by a combination of computational parameters, applied numerical methods and/or boundary conditions but does not suffer from the same practical limitations as physical experiments. For the Reynolds numbers currently achievable, certain aspects of the flow physics observed in physical experiments can be re-examined. Monty and Chong (2009) made a comparison of turbulent channel flow between experimental data and the DNS data of del Álamo et al. (2004) and report some uncertainty as to the ideal box lengths required in DNS to fully and accurately capture the largest scales of motion in turbulent channel and pipe flows and/or issues based on the use of Taylor's hypothesis (see del Álamo and Jiménez 2009; Moin 2009). However, Monty and Chong (2009) notwithstanding, there is little in the way of direct comparison between experimental and numerical data sets. This is due to a lack of well-resolved measurements in channel and pipe flows at comparable Reynolds numbers to the DNS as made clear by Jiménez (2003). The present work was undertaken in an attempt to minimise uncertainties arising from sensor and anemometry parameters, with emphasis placed on spatial resolution issues in order to obtain accurate and reliable measurements of the streamwise velocity component in channel and pipe flows.

1.1 Measurement resolution

One of the most important aspects of measurement uncertainty in wall bounded turbulence, particularly for hot-wire measurements, is the spatial resolution of the measurement probe(s). The seminal work of Ligrani and Bradshaw (1987) addresses the issue of spatial resolution regarding hot-wire measurements of turbulence near walls. By performing a parametric study of hot-wire sensor lengths (l) and length-to-diameter ratios (l/d) in the near-wall region of a turbulent boundary layer, Ligrani and Bradshaw (1987) make the recommendations that for accurate, well-resolved hot-wire measurements, the inner-scaled wire-length $l^+ = lU_\tau/\nu$ should be less than 20 and the length-to-diameter ratio should exceed 200. It must be noted, however, that the measurements from which these recommendations are derived were taken at a single Reynolds number and at a fixed near-wall location in a turbulent boundary layer. Recently, Hutchins et al. (2009) revisited and expanded the findings and recommendations of Ligrani and Bradshaw (1987) and report that insufficient spatial resolution and/or insufficient hot-wire length-to-diameter ratio affects the measured turbulence statistics and energy spectra in a turbulent boundary layer for a large range of Reynolds numbers ($2{,}800 < Re_\tau < 19{,}000$). It was shown that non-constant measurement resolution can mask certain trends in the flow physics. A prevalent example is the Reynolds number dependence of the near-wall peak in streamwise turbulence intensity $\overline{u^2}^+|_m$ (where subscript 'm' denotes the maximum or peak value). Hutchins et al. (2009) report that when spatial resolution is held constant by maintaining a constant inner-scaled wire length, the near-wall peak in turbulence intensity grows with Reynolds

number in a turbulent boundary layer. (Throughout this paper, x, y and z will denote the streamwise, spanwise and wall normal directions, and u, v, and w, their fluctuating velocity components. Capitalisation will denote time-averaged quantities and a superscript '+' will denote viscous or 'inner' scaling.) An insufficient l/d was reported to attenuate the measured energy not only in the near-wall region, but also throughout the log region of the boundary layer. Further, they detail the concept of a maximum flow frequency to highlight the effect of insufficient temporal resolution. In terms of practical guidelines for hot-wire experiments, it was recommended that l^+ be made as small as possible (with $l^+ = 22$ resulting in approximately 10% attenuation of $\overline{u^2}^+|_m$ (Chin et al. 2009)); l/d be greater than 200; and that the measurement system be able to resolve fluctuations with a viscous time scale $t^+ = tU_\tau^2/\nu \lesssim 3$. It is in the light of these new guidelines that this paper documents measurements of internal flows where l^+, l/d and t^+ are controlled in order to distinguish between artefacts owing to these anemometer parameters and physical flow phenomena.

By matching l^+, a direct comparison between channel and pipe flow statistics and energy spectra will not be influenced by spatial resolution effects. Further, the effect of spatial attenuation will be isolated from that of the Reynolds number, which will reveal Reynolds number dependencies that may have otherwise been masked. A direct comparison of channel, pipe and boundary layer flows was previously made by Monty et al. (2009), albeit at a single constant Reynolds number, $Re_\tau = 3{,}000$ and matched $l^+ = 30$. It was reported that the measured u statistics exhibit good similarity in the near-wall and logarithmic regions in all three canonical wall bounded flows, yet significant differences exist in the pre-multiplied u spectra between internal and external flows, even in regions where $\overline{u^2}^+$ are equivalent. The differences in the u spectra between internal and external flows occur in the largest energetic scales which scale on outer variables. There is mounting evidence to suggest that these outer-scaled modes are of great importance, even near the wall. For example, Hutchins et al. (2009) show that it is the increasing contribution of the large scales that causes the inner-scaled turbulence intensity to rise with Reynolds number in a boundary layer flow. Expanding on the findings of Monty et al. (2009), this paper compares channel and pipe flows over the Reynolds number range $1{,}000 \leq Re_\tau \leq 3{,}000$ by comparing mean streamwise velocity statistics and energy spectra.

1.2 Scaling of $\overline{u^2}^+|_m$

One aspect of wall bounded turbulent flows that remains somewhat controversial is the Reynolds number dependence of the near-wall inner-scaled streamwise turbulence intensity, $\overline{u^2}^+$. Whilst it is well established that there exists a peak value and that this peak is located at a wall distance fixed in inner scaling at $z^+ \approx 15 \pm 1$, the behaviour of the peak in $\overline{u^2}^+$, with respect to Reynolds number, is uncertain due to the large variation in the reported magnitude. As previously discussed, Hutchins et al. (2009) report for a turbulent boundary layer that $\overline{u^2}^+|_m$ grows with Reynolds number for a constant measurement resolution. The significant growth of $\overline{u^2}^+|_m$ with Reynolds number for turbulent boundary layers is well supported over a range of Reynolds numbers spanning laboratory to atmospheric flows (see Fernholz and Finley 1996; DeGraaff and Eaton 2000; Metzger and Klewicki 2001; Marusic and Kunkel 2003). In contrast, a survey of the literature conducted by Mochizuki and Nieuwstadt (1996) reports no growth of $\overline{u^2}^+|_m$ for turbulent channel, pipe or boundary layer flows (however, they do not account for spatial resolution issues). Recent measurements by Hultmark et al. (2010) also report that the near-wall peak in turbulence intensity is Reynolds number independent for fully developed turbulent pipe flow at a constant $l^+ \approx 20$; however, l/d and t^+ were allowed to vary in that study. Thus, there remains some ambiguity regarding the measured level of turbulence intensity (see for instance, Morrison and Kronauer 1969; Lawn 1971; Perry and Abell 1975; Morrison et al. 2004; Monty 2005). Further adding to the controversy, channel flow DNS (direct numerical simulation) results in Hoyas and Jiménez (2006) and Jiménez and Hoyas (2008), which have a near constant spanwise resolution, Δy^+, show that $\overline{u^2}^+|_m$ exhibits a Reynolds number dependence for $Re_\tau = 547$, 934 and 2,003, consistent with the findings of Wei and Willmarth (1989). Therefore, in addition to comparing channels and pipes for a range of Reynolds numbers, this paper will also re-examine the Reynolds number dependence of the near-wall peak in turbulence intensity for these internal geometries.

1.3 Scale separation

Also of interest is the energy content and distribution of the flows as they transition from relatively low to relatively high Reynolds numbers because for the modest Reynolds numbers investigated here, not only is the logarithmic region just beginning to emerge, but the separation between inner length scales and outer length scales is also starting to become prominent. This will clearly have implications regarding the large-scale modes (that scale on outer length scales), which populate the logarithmic region, and their contribution towards the measured streamwise turbulence intensity. Following Hutchins and Marusic (2007b), scale separation is deemed sufficient when there is an order of

magnitude separation between inner-scaled energetic modes and outer-scaled energetic modes in terms of inner-scaled wavelength, λ_x^+. The inner-scaled energetic mode is a spectral peak fixed at $z^+ \approx 15$ and $\lambda_x^+ \approx 1,000$, which is universally accepted for turbulent channels, pipes and boundary layers (provided a smooth wall). In a turbulent boundary layer, the outer-scaled mode, termed 'super-structures' in Hutchins and Marusic (2007a), peaks at $\lambda_x \approx 6\delta$; however, in internal flows, there exist two distinct outer-scaled modes termed large-scale motions (LSM) and very-large-scale motions (VLSM), and these modes have characteristic wavelengths of $\lambda_x \approx$ 1–3δ and $\lambda_x \approx 12$–14δ, respectively (see Kim and Adrian 1999; Guala et al. 2006; Balakumar and Adrian 2007; Monty et al. 2007). Accordingly, there are two Reynolds number ranges that would provide an order of magnitude separation between spectral peaks. Considering the longest length scale (VLSM) in a channel or pipe flow is $\lambda_x \approx 14\delta$, the minimum Reynolds number that provides an order of magnitude separation between inner and outer scaled energetic peaks is $Re_\tau \gtrsim 700$. However, when considering the other outer scaled mode (LSM) has a length scale of $\lambda_x \approx 3\delta$, the minimum Reynolds number for sufficient scale separation increases to $Re_\tau \gtrsim 3,300$. Therefore, in this paper, only sufficient scale separation is achieved between the 'inner site' ($\lambda_x^+ \approx 1,000$ energy) and the VLSM ($\lambda_x \approx 14\delta$ energy) for the range of Reynolds numbers investigated here. Separation of all three spectral modes or peaks (if indeed there are three truly independent modes) would require much higher Reynolds numbers. Another consideration is that these outer scaled modes have been shown to exist in the logarithmic region and beyond. If we consider the limits of the logarithmic region to be $100 \leq z^+ \leq 0.15\delta^+$ ($\delta^+ = \delta U_\tau/\nu = Re_\tau$), a logarithmic overlap region only exists for $Re_\tau \gtrsim 667$. Therefore, a decade of overlap region requires the friction Reynolds number to be $Re_\tau \approx 6,667$. The highest Reynolds number investigated in this paper is $Re_\tau = 3,000$, meaning that scale separation on streamwise wavelengths is achieved, but the limited overlap region makes it difficult to separate and clearly identify the energetic modes (and is also the reason for the limited discussion regarding the 'universal' log law constants κ and A in Sect. 3.1.1).

In summary, the aims of this paper are to explore the similarity of channels and pipes over a range of Reynolds numbers, to re-examine the Reynolds number dependence of the near-wall turbulence intensity in internal flows and to provide a database of accurate, well-resolved measurements to facilitate the comparison of physical and numerical experiments in turbulent channels and pipes. Discussion of the individual effects of varying l^+ and l/d on the measured turbulence intensity and energy spectra are a corollary of the matched wire length portion of the study and were necessary to establish the accuracy and consistency of the experiments.

2 Experimental set-up

2.1 Flow facilities

Both the channel flow and pipe flow facilities are located in the Walter Bassett Aerodynamics Laboratory at the University of Melbourne. The channel flow facility is a blower type facility with a working section length of 22 m and a cross-section measuring 1,170 × 100 mm. The 11.7:1 width-to-height ratio ensures two dimensionality of the flow and the long working section ensures that the flow is fully developed. The measurement station was located at $175H$ downstream of the sandpaper trip. Six static pressure taps were used to measure the static pressure gradient and hence provide "direct" measurement of the friction velocity, U_τ. Further details of this flow facility can be found in Monty et al. (2007).

The pipe flow facility is a suction type facility and has a diameter of $D = 98.8$ mm and a working section length of $L = 38.86$ m. This corresponds to a pipe length-to-diameter ratio of $L/D = 393.4$, ensuring that the flow is fully developed. The removable test section was located at $170D$ downstream of the contraction exit. Static pressure taps were spaced at intervals of 6m, and these were used to determine the static pressure gradient. Further details of this facility are available in Perry et al. (1986).

Importantly, these facilities have a nominally equivalent outer length scale, channel half-height $h = 50.0$ mm and pipe radius, $R = 49.4$ mm, and each has a maximum centreline velocity of approximately $U_{cl} \approx 35$ m/s. This allows for a convenient comparison of results obtained from each of these facilities.

2.2 Hot-wire sensor and anemometry details

In order for the hot-wire sensing elements to have both an $l/d > 200$ as recommended by Ligrani and Bradshaw (1987) and a matched inner-scaled wire length of $l^+ = 22$ for a range of Reynolds numbers, the diameter of the Wollaston wire (100% platinum core, silver coating) used to construct the hot-wires ranged from 1.5 to 5.0 μm. The hot-wires were constructed using *Dantec 55P05* and *55P15* boundary-layer type probes with a tip spacing of 3 mm (for 5 μm wires) and 1.25 mm (for 1.5 and 2.5 μm wires), respectively. Having soldered the wires onto the probe tips, the sensing elements were carefully etched to pre-determined lengths to satisfy the matched $l^+ = 22$ criterion. All hot-

wires were inspected after etching and sensing lengths measured with a microscope. For the study of length-to-diameter ratio, the recommendations of Ligrani and Bradshaw (1987) were ignored, and the wires were etched to a constant physical length (l), irrespective of wire diameter (d), thus allowing for a range of l/d ratios at various matched l^+.

All hot-wire probes are operated in constant temperature mode using a custom built Melbourne University Constant Temperature Anemometer (MUCTA II). The overheat ratio was set to 1.8 to provide the maximum frequency response. The system frequency response to a 1-kHz square wave was set to a frequency corresponding to $t^+ \lesssim 1$. This equated to greater than 75 kHz at the highest Reynolds number tested.

The hot-wire probes were calibrated in situ against a Pitot-static probe for both facilities. A third-order polynomial was fitted to the calibration data to obtain hot-wire velocities. For the channel facility, the calibration was carried out at the channel centre-line or channel half-height where turbulence intensities are at a minimum. The Pitot probe and hot-wire were aligned in an external rig to have the same wall normal position, and the probes were offset in the spanwise direction by 10 mm. The hot-wire was aligned to be parallel to the wall and the initial wall normal location of the hot-wire is measured using a microscope. A *Renishaw* linear optical encoder with 0.5-μm resolution was used to determine the location of the probe relative to the initial wall normal location. The encoder was used throughout the traversing measurement and hot-wire calibration procedure.

Calibration of the hot-wire sensors in the pipe flow was also carried out in situ. The pipe test section was removed, the hot-wire aligned and the initial wall normal position determined by a microscope. However, pipe flows do not possess the two dimensionality of channel flows, and the Pitot probe was offset from the hot-wire probe in the wall normal direction. The offset of the two sensors was measured before the test section was placed back into the facility. Since the mean velocity profile of the pipe flow is symmetrical and the velocity gradients are shallow in the core of the flow, hot-wire calibration can be carried out by ensuring the hot-wire and Pitot-tube anemometers are placed equidistant about the pipe centreline. The same *Renishaw* linear optical encoder was used to determine the location of the hot-wire sensor during calibration and measurement.

For all experiments, an *MKS Baratron 698A11TRA* differential pressure transducer and *MKS Type 270* signal conditioner were used to measure the pressures from the Pitot-static probe during calibration and the traversing measurements as well as measuring the static pressure gradient in the flow facility. The temperature and atmospheric pressure were measured using a calibrated thermocouple and a *Sensortechnics* 144S-BARO barometer. All signals were sampled using a *Data Translation* DT-9836 16-bit data acquisition board. Hot-wire signals were sampled at an interval of $\Delta t^+ \lesssim 0.5$ to ensure that smallest energetic scales were captured. Full details of the experimental conditions and sensor parameters are provided in Table 1. An uncertainty analysis was carried out using the standard method described in Kline and McClintock (1953), and these estimates are given in Table 2. The hot-wire uncertainties are consistent with previous analyses for well-calibrated hot-wires as reported by Yavuzkurt (1984), Bruun (1995) and Jorgensen (1996).

3 Mean streamwise velocity statistics

Mean statistics of streamwise velocity from the channel and pipe flow for matched Kàrmàn numbers of $Re_\tau = 1{,}000$, 2,000 and 3,000 are presented in this section. Section 3.1 present the mean velocity and turbulence intensity profiles measured using a matched $l^+ = 22$, and therefore a constant spatial resolution. Section 3.2 provides a comparison to channel flow DNS at $Re_\tau = 2{,}000$, and Sect. 3.3 examines the various effects of l^+ and l/d on the measured statistics.

3.1 Mean flow statistics for $l^+ = 22$

This section presents measurements where the hot-wire spatial resolution was held constant at $l^+ = 22$ and $l/d \gtrsim 200$. These particular cases are noted in Table 1 and allow direct comparison between channel and pipe flows unbiased by measurement parameters.

3.1.1 Mean velocity

The mean velocity profiles from each geometry are plotted together for comparison in Fig. 1, with plots a and b being channel flow mean velocity and velocity deficit profiles and plots c and d the corresponding pipe flow profiles. The channel and pipe flow data presented here were found to be in good agreement with a logarithmic law of the wall with 'universal' constants κ and A defined as,

$$U^+ = \frac{1}{\kappa}\ln(z^+) + A, \tag{1}$$

where $\kappa = 0.39$ and $A = 4.42$ for the channel flow and $\kappa = 0.38$ and $A = 4.23$ for the pipe flow. The constants for all measurements were determined by performing a linear regression for all data points that lie within the range

Table 1 Experimental conditions and hot-wire sensor parameters for all experiments

Facility	U_{cl}	Re_τ	d (μm)	l (mm)	l^+	l/d	Δt^+	f_s (kHz)	T (s)	TU_{cl}/δ
Channel	7.13	1,049	1.5	0.356	7.5	237	0.04	150	60	8,554
Channel	7.14	1,024	2.5	0.567	11.6	227	0.13	50	180	25,686
Channel	7.43	1,053	5.0	1.040	21.9†	208	0.07	100	150	22,290
Channel	15.55	2,019	1.5	0.346	14.0	231	0.44	60	60	18,660
Channel	15.55	2,072	2.5	0.538	22.3†	216	0.26	100	120	37,320
Channel	15.61	2,070	5.0	1.190	49.4	238	0.44	60	60	18,727
Channel	23.71	3,026	1.5	0.346	21.0†	231	0.47	120	30	14,227
Channel	23.49	3,006	2.5	0.540	32.5	216	0.47	120	90	42,296
Channel	23.69	3,035	5.0	1.190	72.4	238	0.49	120	30	14,212
Pipe	7.68	1,023	1.5	0.366	7.6	244	0.22	30	150	23,305
Pipe	7.59	1,037	2.5	0.575	12.1	230	0.45	15	150	23,056
Pipe	7.63	1,046	5.0	1.040	22.0†	208	0.46	15	120	18,525
Pipe	16.64	2,044	1.5	0.366	15.1	244	0.45	60	60	20,207
Pipe	16.35	2,002	2.5	0.575	22.4†	230	0.43	60	60	19,852
Pipe	16.15	2,026	5.0	1.040	42.6	208	0.43	60	60	19,615
Pipe	25.47	2,984	1.5	0.366	22.1†,‡	244	0.49	120	45	23,205
Pipe	25.30	3,035	2.5	0.575	35.4	230	0.48	120	30	15,363
Pipe	25.32	3,069	5.0	1.020	63.4	204	0.49	120	45	23,063
Pipe	7.50	1,022	5.0	0.385	7.90	77	0.22	30	150	22,782
Pipe	16.25	2,039	5.0	0.385	15.9	77	0.43	60	90	29,609
Pipe	25.42	3,056	5.0	0.385	22.6‡	77	0.49	120	45	23,159
Pipe	7.52	1,046	2.5	0.365	7.7	146	0.23	30	150	22,840
Pipe	16.67	2,090	2.5	0.365	15.5	146	0.46	60	90	30,372
Pipe	24.87	3,019	2.5	0.365	22.3‡	146	0.48	120	45	22,653
Pipe	7.77	1,055	1.0	0.365	7.8	365	0.24	30	120	18,879
Pipe	16.37	2,018	1.0	0.365	14.7	365	0.44	60	60	19,877
Pipe	25.06	3,002	1.0	0.365	22.2‡	365	0.48	120	45	22,831

† Matched l^+ data and ‡ matched Re_τ and l^+ for varying l/d

Table 2 Uncertainty estimates

Source	Uncertainty
Pressure transducer	±0.15%
Temperature	±0.2%
Atmospheric pressure	±0.1%
Friction velocity, U_τ	±1%
Pitot probe uncertainty during calibration	±0.5%
Wire size, l	±0.038 mm
Initial wall normal position	±0.025 mm
Wall normal position over profile	
Channel	±0.015 mm/m
Pipe	±0.025 mm/m
Hot-wire measurement of	
Inner scaled mean velocity, U^+	≈±2%
Inner scaled turbulence intensity, $\overline{u^2}^+$	≈±4%

$100 \lesssim z^+ \lesssim 0.15\delta^+$. Although there exists some ongoing controversy regarding the universality of the log law constants and values vary throughout the literature (see Zagarola and Smits 1998; Perry et al. 2001; Zanoun et al. 2003; McKeon et al. 2004; Buschmann and Gad-el-Hak 2009; Marusic et al. 2010), the values reported here come from a curve fit to the new data only and are consistent with other findings at low to moderate Reynolds numbers (see Nagib and Chauhan 2008). Importantly, for this limited Reynolds number range, there exists only a limited overlap region, and hence, the values of κ and A become very sensitive to the chosen log region limits. The mean velocity profiles were also shown to agree with traditional constants of $\kappa = 0.41$ and $A = 5.0$, to within experimental error (also plotted in Fig. 1a, c). Thus, it is clear that conclusions regarding universal scaling of the mean velocity cannot be drawn from data at these relatively low Reynolds numbers. Therefore,

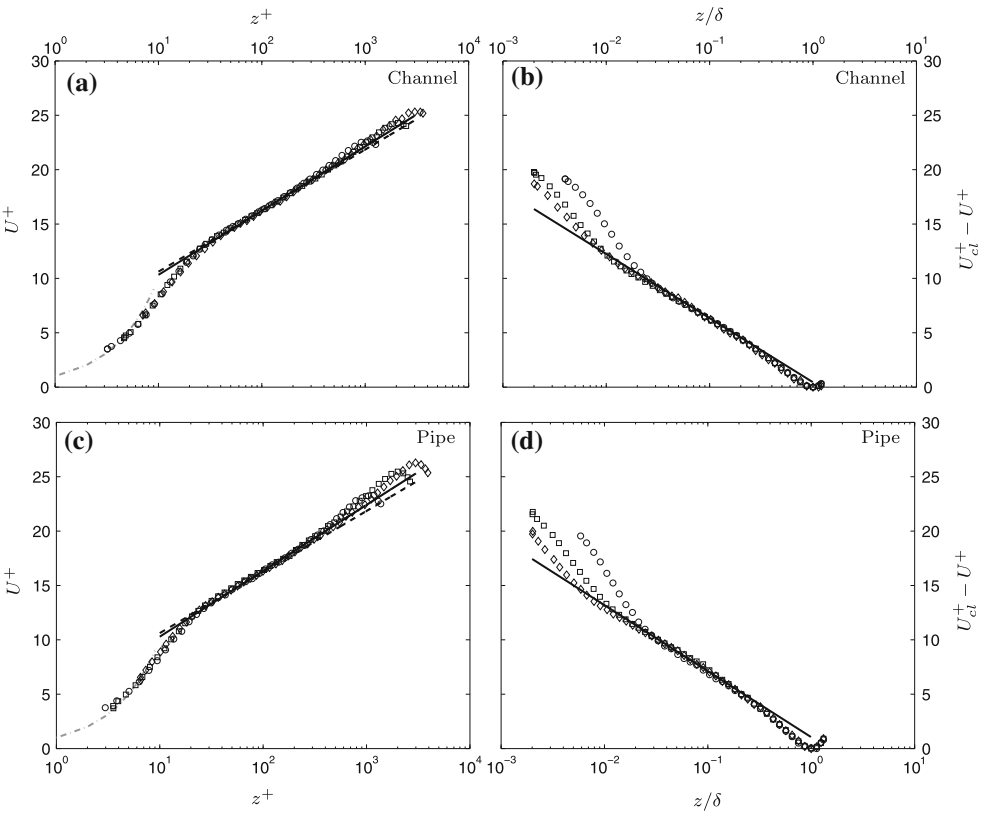

Fig. 1 **a** Channel flow mean velocity profiles for $Re_\tau \approx 1{,}000$ (*open circle*), 2,000 (*open square*) and 3,000 (*open diamond*) at matched $l^+ = 22$. *Solid line* is Eq. 1 where $\kappa = 0.39$ and $A = 4.42$, *dashed line* $\kappa = 0.41$ and $A = 5.0$; *dot-dashed line* $U^+ = z^+$. **b** Corresponding velocity deficit profiles. *Solid line* is Eq. 2 where $\kappa = 0.39$ and $B = 0.44$. **c** Pipe flow mean velocity profiles for $Re_\tau \approx 1{,}000$ (*open circle*), 2,000 (*open square*) and 3,000 (*open diamond*) at matched $l^+ = 22$. *Solid line* is Eq. 1 where $\kappa = 0.38$ and $A = 4.23$, *dashed line* $\kappa = 0.41$ and $A = 5.0$; *dot-dashed line* $U^+ = z^+$. **d** Corresponding velocity deficit profiles. *Solid line* is Eq. 2 where $\kappa = 0.38$ and $B = 1.04$

the mean velocity data presented here are not an attempt to re-examine the values of κ and A, but rather to establish the collapse of this statistic before presenting the second-order statistics and energy spectra.

For the inner-scaled profiles (Fig. 1a, c), both geometries exhibit similarity in the near-wall and logarithmic regions and only deviate in the outer or wake regions. Another method to examine the mean velocity distribution is to consider the mean relative velocity, or the velocity deficit. This is defined as

$$U_{\mathrm{cl}}^+ - U^+ = -\frac{1}{\kappa}\ln\left(\frac{z}{\delta}\right) + B, \tag{2}$$

where again κ is 'universal' and, however, B is geometry dependent. A linear regression was performed on the velocity deficit data to yield constants of $B = 0.44$ for the channel flow and $B = 1.04$ for the pipe flow. The different values of B highlight the different 'wake strength' present in the flow in each geometry. This is consistent with findings by Monty et al. (2009), where it was noted that 'wake strength', or deviation from the logarithmic law is strongest for zero-pressure gradient flat plate boundary layer, then pipes and then channels.

3.1.2 Turbulence intensity

Figure 2 presents the wall normal profiles of streamwise turbulence intensity. Since all measurements were taken using hot-wires with matched inner-scaled sensor lengths ($l^+ = 22$), the behaviour of the streamwise turbulence intensity is isolated from attenuation due to sensor size. An inspection of these plots reveals that channel and pipe flow streamwise turbulence intensity profiles exhibit close similarity across the entire profile for Reynolds numbers up to $Re_\tau = 3{,}000$, in agreement with Monty et al. (2009). Further, it is clear that the near-wall peak in turbulence intensity rises with Reynolds number in both channels and pipes contrary to what has previously been reported in the literature. The total rise in $\overline{u^2}^+|_m$ is approximately 14%, which far exceeds the ±4% error typically associated with hot-wire measurements of turbulence intensity. This growth in $\overline{u^2}^+|_m$ was also observed for profiles where Reynolds number increased from $Re_\tau = 1{,}000$ to 2,000, measured using a near-constant sensor length of $12 \leq l^+ \leq 15$ (see Table 1), although these data were not plotted for brevity.

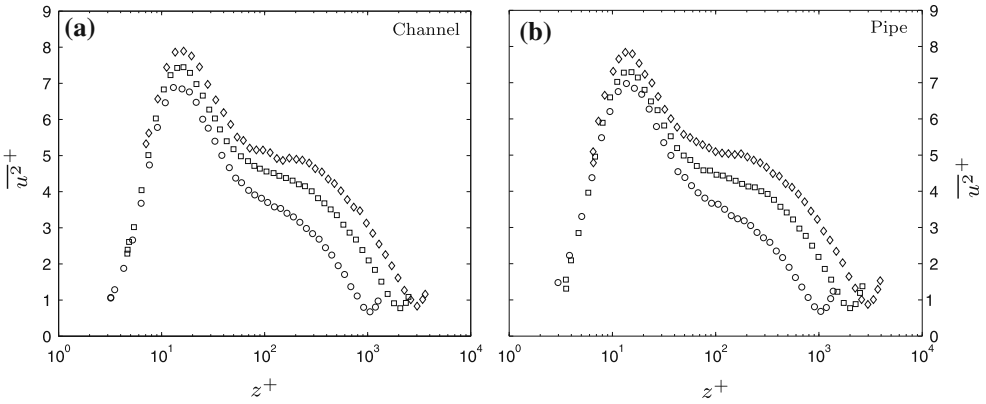

Fig. 2 **a** Channel flow turbulence intensity profiles at $Re_\tau \approx 1{,}000$ (*open circle*), 2,000 (*open square*) and 3,000 (*open diamond*). **b** Pipe flow turbulence intensity at matched Reynolds numbers. All profiles: $l^+ = 22$

Also of note is the rapid decay in turbulence intensity throughout the log region $(100 \lesssim z^+ \lesssim 0.15\delta^+)$ for both channel and pipe flows at the lowest Reynolds number. The profiles exhibit a very rapid, almost logarithmic decay spanning the entire log region at $Re_\tau = 1{,}000$. For $Re_\tau = 2{,}000$, the apparently logarithmic decay again spans the log region, yet it is much less rapid. However, at the higher Reynolds number, the turbulence intensity does not appear to decay in a logarithmic fashion. The profile appears to plateau over a very narrow region near the geometric midpoint of the logarithmic region. Mathis et al. (2009a, b) identified the midpoint of the logarithmic region to be located at $z^+ \approx 3.9\sqrt{Re_\tau}$, and this point is tracked on turbulence intensity profiles at various Reynolds numbers (shown later in Fig. 10c). This observed plateau and the rise in turbulence intensity for a given value of z^+ at increasing Reynolds numbers were predicted in the flat plate boundary layer turbulence intensity formulations of Marusic et al. (1997) and Marusic and Kunkel (2003) and are consistent with Townsend's attached eddy hypothesis. Hutchins et al. (2009) show that for a turbulent boundary layer, the turbulence intensity rising in the logarithmic region is due to the increasing contribution of the large scales of motion. Indeed, the rise in turbulence intensity throughout even the near-wall region is due to the large scales. (The relative contribution of scales and their effect on the measured turbulence intensity over the Reynolds number range will be discussed at length in Sect. 4).

3.2 Comparing with channel flow DNS at $Re = 2{,}000$

A detailed comparison of the streamwise mean statistics and energy spectra from the channel facility used in this paper and the channel flow DNS data of del Álamo et al. (2004) was previously made by Monty and Chong (2009) for a friction Reynolds number of $Re_\tau \approx 1{,}000$. Here, comparison will be made with the mean flow statistics at $Re_\tau \approx 2{,}000$ for the channel flow DNS data published in Hoyas and Jiménez (2008) and Jiménez and Hoyas (2008). Comparing data sets, whether between different flow geometry or between physical and numerical experiments, is ideally done by matching as many parameters as possible (for example; Reynolds number, spatial and temporal resolution). One way to achieve this when comparing hot-wire data and DNS data is to build a hot-wire small enough to match the resolution of the DNS. This was not possible with the facilities available during this study. A much simpler method is to filter the DNS data to match the viscous scaled wire length assuming that $\Delta y^+ \simeq l^+$ (see Chin et al. 2009). This solution, though simpler, requires access to volumetric channel flow DNS data sets at $Re_\tau = 2{,}000$. These were not publicly available at the time of writing. Therefore, the following comparison of physical and numerical channel flow is not a *direct* one in the strictest sense as only the flow Reynolds number is matched.

Figures 3a, b present channel flow mean velocity and turbulence intensity profiles where the solid black symbols are DNS data and hollow symbols are hot-wire data at $Re_\tau = 2{,}000$. The DNS data have an inner-scaled spanwise resolution of $\Delta y^+ = 6.1$ and the hot-wire data were acquired with wire lengths of $l^+ = 14.0$, 22.3 and 49.4. All experimental mean velocity profiles display very good agreement with those of the DNS. However, the turbulence intensity profiles only collapse for all four cases in the outer region. The near-wall peak in the turbulence intensity is highest for the DNS data as it has a superior spanwise spatial resolution to that of the hot-wire (assuming $\Delta y^+ \simeq l^+$). For the hot-wire measurement where a sensor of $l^+ = 14$ was employed, the turbulence intensity agrees well with the DNS throughout the logarithmic and outer regions and displays an attenuated peak owing to inferior spatial resolution. It is clear that the turbulence intensity profiles are increasingly attenuated with increasing sensor size and this effect will be discussed further in Sect. 3.3. For now, it can be concluded that the hot-wire measurements agree well with the DNS in first- and second-order statistics with discrepancies in the turbulence intensity

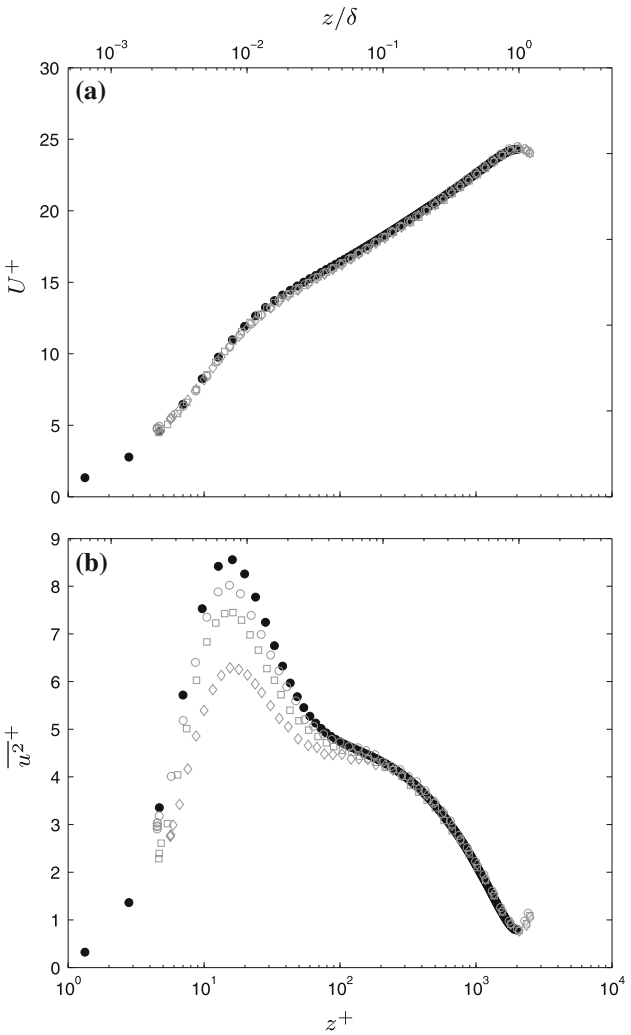

Fig. 3 Comparison of channel flow experiment with DNS at $Re_\tau \approx 2{,}000$. **a** Mean velocity and (**b**) turbulence intensity profiles. *Black solid symbols* represent DNS data and *grey hollow symbols* represent hot-wire measurements. (*filled circle*) DNS $\Delta y^+ = 6.1$, (*opencircle*) $l^+ = 14.0$, (*opensquare*) $l^+ = 22.3$ and (*open diamond*) $l^+ = 49.4$

profiles owing to the varying spatial resolution of the data sets.

3.3 Effect of hot-wire sensor length on measured turbulence intensity

The hot-wire measured turbulence intensity is a complex function of spatial resolution and Reynolds number. For a fixed outer length scale, such as the channel half-height or pipe radius, small scales become increasingly small as the Reynolds number increases. The implication is that the effective length of a given hot-wire sensor increases with increasing Reynolds number, leading to higher levels of attenuation. Ligrani and Bradshaw (1987) recommended that l/d should be no less than 200, therefore, to maintain a constant spatial resolution, and a different sensor must be used for each Reynolds number. This is practically very difficult to achieve as commercially available wire diameters are limited and decreasing wire diameters makes for increasingly fragile sensors. Typically, in hot-wire measurements, spatial resolution is either not controlled or the length-to-diameter ratio is relaxed. This does not mean that data acquired as such are not useful, only that anemometry parameters must be considered before making comparisons. In the following paragraphs, two of the parameters relevant to hot-wire measured fluctuating velocity are systematically examined with the purpose of demonstrating the different effect of each parameter on the measured turbulence intensity. Although the following sections are limited to hot-wire measurements, spatial resolution issues exist in other measurement techniques (e.g. interrogation volumes in PIV and LDV) and some of the insights from the following discussion may be useful in analysis of those data.

3.3.1 *Varying l^+ with varying Re_τ*

Figure 4 plots turbulence intensity profiles at matched Reynolds numbers measured using two wires of fixed physical lengths, which means l^+ is allowed to vary. Figure 4a shows profiles measured using a 5-μm-diameter hot-wire, and Fig. 4b shows profiles measured using a 1.5-μm-diameter hot-wire. In order to keep $l/d \geq 200$, the corresponding sensor lengths were made to $l \approx 1$–1.2 mm and $l \approx 0.34$–0.35 mm. Figure 4 shows that when not controlling for spatial resolution, the measured streamwise turbulence intensity profiles vary markedly. Indeed, one may conclude from Fig. 4a that the near-wall turbulence intensity decreases with increasing Reynolds number, yet Fig. 4b appears contradictory, showing a constant near-wall peak in turbulence intensity. In fact, both conclusions are misleading as both cases have non-constant spatial resolution (Recall Fig. 2 for turbulence intensities at constant spatial resolution).

It is obvious that the smaller the sensor length, the more resolved the measurement. Figure 4a, b clearly highlight the competing effects of increasing Reynolds number and increasing spatial attenuation (for a fixed l). For the large sensor in Fig. 4a, the increasing turbulence intensity is dominated by the attenuation due to increasing sensor length. In Fig. 4b, these competing effects strike a balance and the near-wall turbulence intensity appears constant for $1{,}000 \leq Re_\tau \leq 3{,}000$. Therefore, by not accounting for increasing sensor lengths, the Reynolds number dependence of the turbulence intensity is masked, or for more extreme sensor sizes, the increasing attenuation simply overwhelms the effect of increasing Reynolds number.

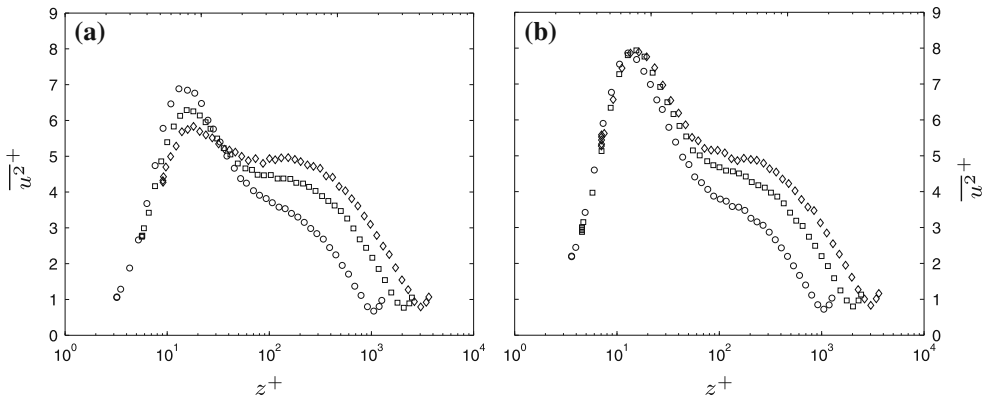

Fig. 4 Channel flow turbulence intensity profiles for $Re_\tau \approx 1{,}000$ (*open circle*), 2,000 (*open square*) and 3,000 (*open diamond*). **a** Fixed hot-wire sensor length $l \approx$ 1.04–1.19 mm. Corresponding $l^+ \approx$ 22 (*opencircle*), 49 (*opensquare*) and 72 (*open diamond*). **b** Fixed hot-wire sensor length $l \approx$ 0.34–0.35 mm. Corresponding $l^+ \approx$ 7 (*opencircle*), 14 (*opensquare*) and 21 (*open diamond*)

Interestingly, the profiles in Fig. 4b are measured using a inner-scaled wire length of approximately 20 or less. The constant magnitude of $\overline{u^2}^+|_m$ in Fig. 4 challenges the recommendation of Ligrani and Bradshaw (1987) that $l^+ = 20$ is small enough because there is still appreciable attenuation even for $7 \leq l^+ \leq 21$. This was also demonstrated by the attenuation in the turbulence intensity between the DNS ($\Delta y^+ = 6.1$) and hot-wire ($l^+ = 14.0$) as discussed in Sect. 3.2.

3.3.2 *Effects of spatial resolution: varying l^+ with fixed Re_τ*

By holding the Reynolds number constant and making measurements with a variety of sensor sizes, one can gain some insight into the attenuation due to sensor length isolated from the competing Reynolds number effect. Figure 5a, b show the mean velocity and turbulence intensity profiles from channel flow at $Re_\tau = 3{,}000$. The mean velocity profiles do not appear affected by spatial resolution, with good similarity displayed by all three profiles. The turbulence intensity profiles, however, clearly exhibit a systematic attenuation of the near-wall peak with increasing inner-scaled wire length, l^+. In fact, it is not only the near-wall peak that is diminished with increasing l^+, as the turbulence intensity profiles only exhibit similarity for $z^+ \gtrsim 300$ at $Re_\tau = 3{,}000$. The collapse of the turbulence intensity profiles for increasing z^+ appears to be dependent on l^+ and Re_τ. Examination of all the turbulence intensity profiles measured for this paper, which includes sensor sizes ranging from $7 \lesssim l^+ \lesssim 73$, reveals that with increasing sensor size, attenuation of the measured turbulence intensity profile extends further and further from the wall. This finding is consistent with Chin et al. (2009) where spatial resolution issues were examined by filtering DNS channel flow data at $Re_\tau = 934$.

Hutchins et al. (2009) show that for a boundary layer flow at $Re_\tau = 14{,}000$ and $l^+ = 153$, not only is the energy signature of the near-wall cycle absent, the reduction in the measured energy can extend through the entire logarithmic region. This missing energy causes a reduction in turbulence intensity, and it was shown that insufficient spatial resolution may be the cause of the appearance of an 'outer hump' in the turbulence intensity profile as reported by Morrison et al. (2004). Figure 4a suggests that as the sensor size becomes increasingly large, the near-wall peak in turbulence intensity is diminished and an outer hump in turbulence intensity begins to appear, which is consistent with the findings of Hutchins et al. (2009). However, as the data presented by Morrison et al. (2004) are at a Reynolds number an order of magnitude higher than the data in this paper, it is not possible to suggest that their finding of an outer hump is entirely due to spatial resolution issues. Confirmation of such hypotheses will require new, highly resolved measurements at very high Reynolds number internal flows with a constant spatial resolution or very small probes.

3.3.3 *Effects of hot-wire length-to-diameter ratio: fixed l^+ and Re_τ with varying l/d*

Figure 6a, b show the mean velocity and turbulence intensity profiles from pipe flow at $Re_\tau = 3{,}000$ and a matched $l^+ = 22$. Here, the length-to-diameter ratio is allowed to vary and has values of $l/d = 77$, 146, 244 and 365. Again, mean velocity appears unaffected with good collapse to within the experimental error of hot-wire measurements. However, plots of turbulence intensity reveal diminished broadband intensity profiles right across the flow for $l/d = 77$ and 146, while the turbulence intensity profiles for $l/d = 244$ and 365 appear to be the same to within the expected error of approximately ±4%.

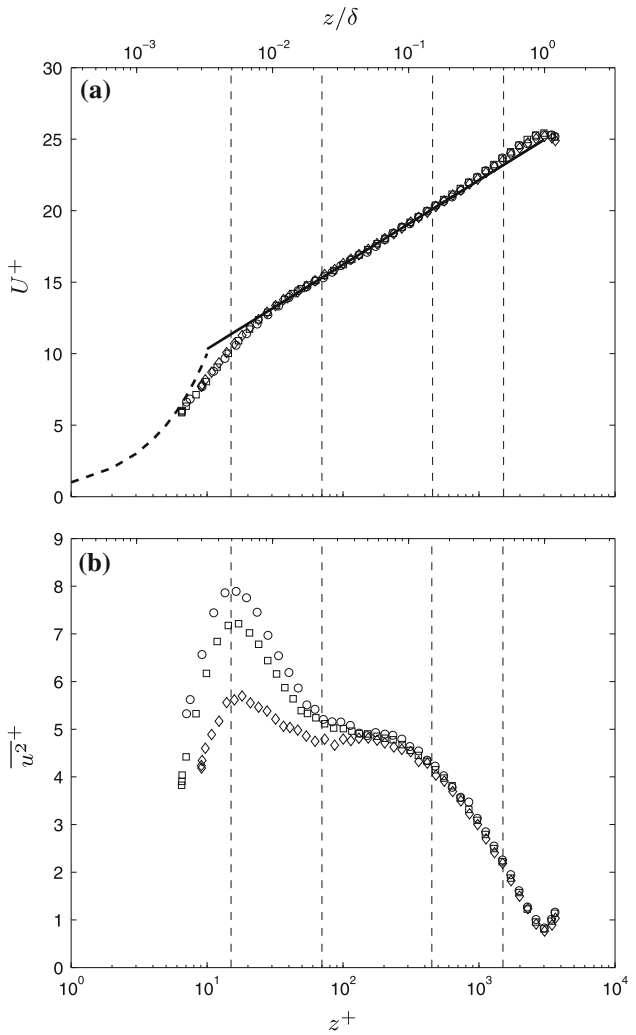

Fig. 5 **a** Mean velocity profiles of fully developed turbulent channel flow at $Re_\tau = 3{,}000$. **b** Corresponding turbulence intensity profiles. Inner-scaled wire lengths: (*open circle*) $l^+ = 21$; (*opensquare*) $l^+ = 35$; (*open diamond*) $l^+ = 72$. *Solid line* is $U^+ = \kappa^{-1}\ln(z^+) + A$ where $\kappa = 0.39$ and $A = 4.42$; *dashed line* $U^+ = y^+$. *Vertical dashed lines* indicate wall normal positions of $z^+ = 15$, 70, $0.15\delta^+$ and $0.5\delta^+$

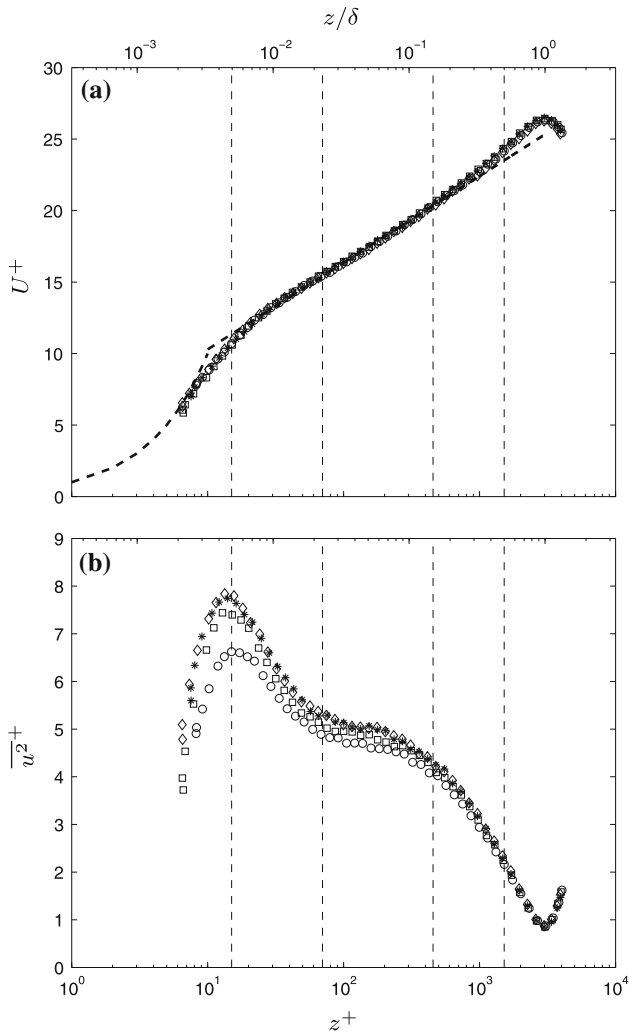

Fig. 6 **a** Mean velocity and **b** turbulence intensity profiles for pipe flow at $Re_\tau = 3{,}000$ for matched inner-scaled wire length of $l^+ = 22$. (*opencircle*) $l/d = 77$, (*opensquare*) $l/d = 146$, (*opendiamond*) $l/d = 244$ and (*asterisk*) $l/d = 365$. *Solid line* is $U^+ = \kappa^{-1}\ln(z^+) + A$ where $\kappa = 0.38$ and $A = 4.23$; *dashed line* $U^+ = y^+$. *Vertical dashed lines* indicate wall normal positions of $z^+ = 15$, 70, $0.15\delta^+$ and $0.5\delta^+$

These findings are consistent with those reported for boundary layers by Hutchins et al. (2009). The diminished turbulence intensity well into the outer region would suggest that an insufficient *l/d* causes a different kind of attenuation than that caused by insufficient spatial resolution. Where attenuation due to long sensors is scale dependent, akin to spatial averaging, it appears that the attenuation caused by *l/d* effects occurs over a much broader range of wavelengths. (These results will be presented in an examination of the energy spectrum in Sect. 4.2.3).

Figure 7 plots the magnitude of the near-wall peak in turbulence intensity (from Fig. 6b) as a function of *l/d* ($Re_\tau = 3{,}000$ and $l^+ = 22$) compared to data from Hutchins et al. (2009) ($Re_\tau = 14{,}000$ and $l^+ = 22$). These data are at a matched l^+, measured using hot-wire sensors constructed in an identical manner. The two curve fits show good agreement except for the data from Hutchins et al. (2009) reaching a higher asymptotic value of $\overline{u^2}^+|_m$, which is expected because of the higher Reynolds number. Selected data from Ligrani and Bradshaw (1987) ($Re_\tau \approx 1{,}000$ and $l^+ \leq 10$) are also plotted for comparison. The line of best fit to the data from Ligrani and Bradshaw (1987) is different in shape to the curve fits for the data presented here and the data from Hutchins et al. (2009). The cause of the discrepancy is unclear, but may be due to the combined effects of spatial resolution (which was shown by Chin et al. (2009) to have effects even for

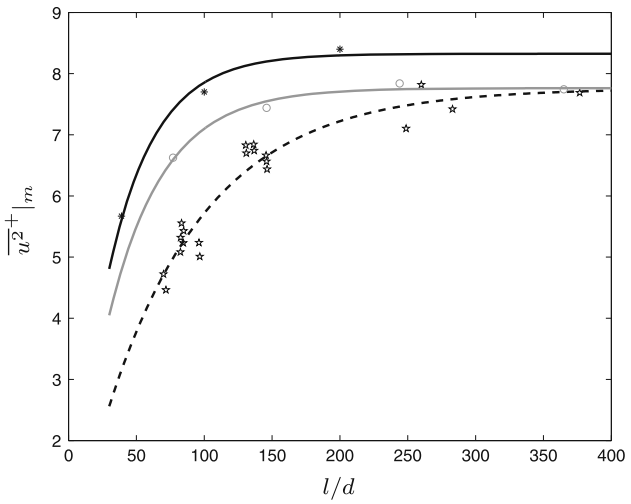

Fig. 7 Variation of near-wall peak in turbulence intensity, $\overline{u^2}^+|_m$, as a function of hot-wire probe length to diameter ratio (l/d). (*Star*) are from Ligrani and Bradshaw (1987) for $Re_\tau \approx$ 1,000 and $l^+ \leq 10$. (*Asterisk*) are from Hutchins et al. (2009) for $Re_\tau \approx$ 14,000 and $l^+ = 22$. (*Open circle*) are from current study for $Re_\tau = 3{,}000$ and $l^+ = 22$. *Lines* show best fit to the data using a form $\overline{u^2}^+|_m = B(1 - \exp A(l/d))$

$l^+ \leq 10$) and the nature of hot-wire end conduction effects, which is dependent on the wire material and stub geometry. It is worth noting that the subminiature probes used in Ligrani and Bradshaw (1987) had a different geometry and used different wire material (90% platinum, 10% rhodium) to the probes used in Hutchins et al. (2009) and this study.

Li et al. (2004) conducted a numerical study of the steady-state heat balance equation for a hot-wire and support stubs and showed that the temperature profile across a hot-wire is dependent on l/d, the stub length, the wire materials and the wire Reynolds number ($Re_w = Ud/\nu$). It was shown that for a given ratio of heat loss due to end conduction versus total heat loss due to end conduction and forced convection, defined as σ, the minimum allowable l/d is heavily dependent on Re_w. Choosing $\sigma \leq 7\%$, Li et al. (2004) show that l/d for platinum wires need only be greater than 200 for $Re_w = \mathrm{O}(10)$, which corresponds to typical velocities in laboratory experiments in atmospheric conditions. Here, hot-wire Reynolds numbers over a wall normal distance of $15 \leq z^+ \leq 3{,}000$ range from $3.32 \leq Re_w \leq 8.17$ ($l/d = 77$), $1.62 \leq Re_w \leq 4.04$ ($l/d = 146$), $1.00 \leq Re_w \leq 2.38$ ($l/d = 244$) and $0.63 \leq Re_w \leq 1.61$ ($l/d = 365$). Given this range of wire Reynolds numbers, the findings in this section are consistent with Li et al. (2004) and this brief discussion serves to highlight the differences the effect of l^+ and l/d have on the measured statistics. Note also that the data where inner scaled wire length was matched at $l^+ = 22$, presented in Sect. 3.1.2 have a wire Reynolds number at $z^+ = 15$ ranging from $1.00 \lesssim Re_w \lesssim 1.10$; hence, the wire Reynolds number effect on the measured $\overline{u^2}^+|_m$ is negligible.

A full experimental study of hot-wire l/d ratios and end effects for a matched l^+ is practically prohibitive because the currently available range of wire diameters is limited. For now, the results support both Ligrani and Bradshaw (1987) and Li et al. (2004) in that $l/d \geq 200$ appears to be both necessary and sufficient for pure platinum wires in the flow regime reported here. However, as a cautionary note for future work, it may be prudent to consider these sometimes overlooked anemometer parameters as different wire materials and stub geometries will have different dynamic conduction properties.

4 Pre-multiplied energy spectra of streamwise velocity

4.1 Energy spectra for $l^+ = 22$

The one-dimensional pre-multiplied energy spectra of streamwise velocity for channel and pipes flows at $Re_\tau = 1{,}000$, 2,000 and 3,000 for a matched wire length of $l^+ = 22$ are presented together in Fig. 8. These iso-contours show the pre-multiplied u spectra ($k_x\phi_{uu}/U_\tau^2$) as a function of streamwise wavelength (λ_x^+ or λ_x/δ) and wall normal position (z^+ or z/δ). Spatial information is inferred from the time series data using Taylor's hypothesis (Taylor 1938) with streamwise wavelengths estimated using the local mean velocity. Dennis and Nickels (2008) demonstrated the accuracy of Taylor's hypothesis using the local mean velocity for projection distances of up to $x = 6\delta$ in the logarithmic region. However, it has recently been shown that the convection velocity is scale dependent (see del Álamo and Jiménez, 2009; Monty and Chong 2009; Chung and McKeon 2010). While the choice of convection velocity will change the shape of the spectra in Fig. 8, these changes will not affect the conclusions of this study concerning Reynolds number dependence, spatial resolution effects or the comparison of channel and pipe flows. The channel and pipe flows appear to be very similar in energy content and are effectively the same within experimental uncertainty. Generally, the internal flows have been shown to possess three predominant energetic modes, each attributed to recognised coherent flow features. One mode is at a fixed position with inner scaling ($z^+ \approx 15, \lambda_x^+ \approx 1{,}000$) and a fixed magnitude for a given wire length l^+, and represents the energy contribution of the near-wall cycle of counter-rotating quasi-streamwise aligned vortical structures first reported in Kline et al. (1967) as characteristic streaks in the velocity field of the near-wall region of a turbulent boundary layer. Kim and Adrian (1999) identified two other modes that exist in the

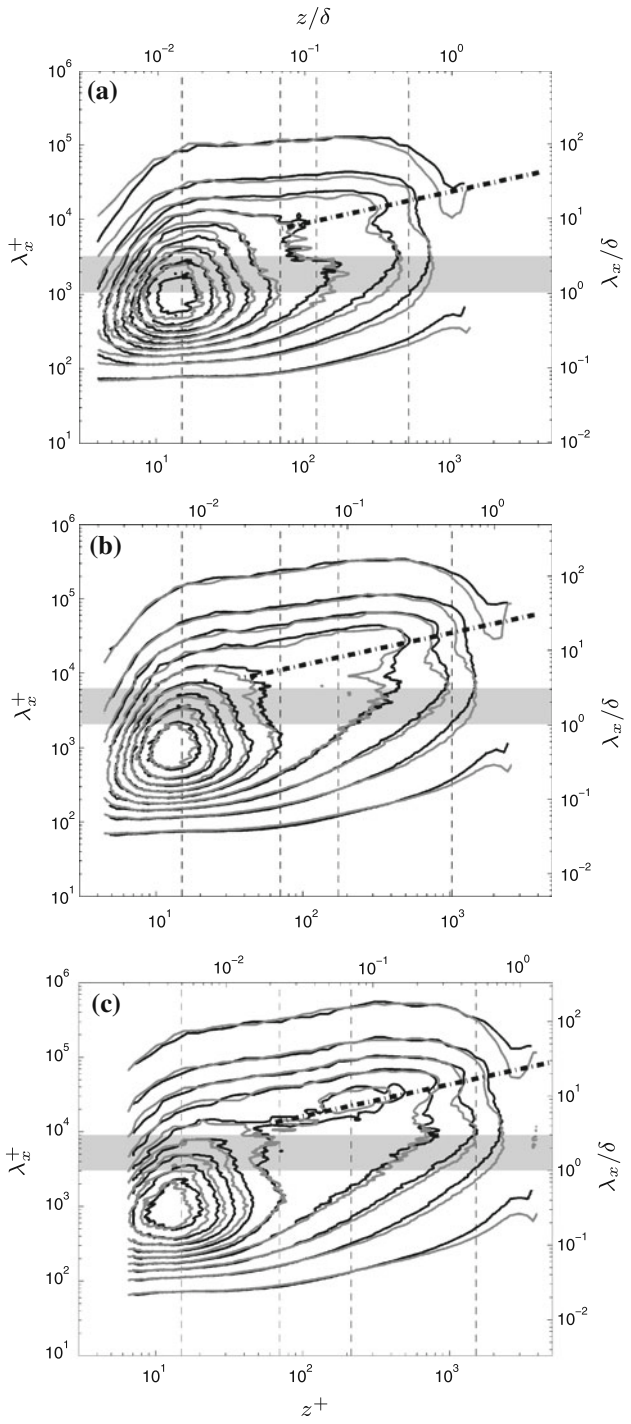

Fig. 8 Contours of u spectra for **a** $Re_\tau = 1{,}000$, **b** $Re_\tau = 2{,}000$ and **c** $Re_\tau = 3{,}000$ at a matched $l^+ = 22$. Channel (*black*), pipe (*grey*). Contour levels are from $k_x\phi_{uu}/U_\tau^2 = 0.1$ to 1.7 in increments of 0.2. *Vertical dashed lines* indicate wall normal positions of $z^+ = 15, 70, 3.9\sqrt{Re_\tau}$ and $0.5\delta^+$. *Shaded area* indicates LSM ($1 \le \lambda_x/\delta \le 3$) and the *heavy dot-dashed line* represents VLSM growth according to Eq. 3

logarithmic region and beyond for pipe flows. These modes were shown to scale with δ and appear at wavelengths of $\lambda_x \approx 1 - 3\delta$ and $\lambda_x \approx 12 - 14\delta$, are the large-scale motions (LSM) and very-large-scale motions (VLSM), respectively. The LSM and VLSM were also shown to exist in channel flows by Balakumar and Adrian (2007) and Monty et al. (2007) among others. The VLSM appear to grow in length throughout the logarithmic region, and Monty et al. (2009) suggest that this growth follows a power law:

$$\frac{\lambda_x}{\delta} = 23\left(\frac{z}{\delta}\right)^{\frac{3}{7}}, \tag{3}$$

which is plotted as a dot-dashed line in Fig. 8a–c and shows good agreement with the data presented here. In contrast, Hutchins and Marusic (2007b) show only a single energetic peak at $\lambda_x \approx 6\delta$ for boundary layer flows and also noted that the bi-modal distribution of the boundary layer u spectrum is not as apparent at low Reynolds numbers due to an insufficient scale separation and a short logarithmic overlap region. However, it was noted by Hutchins and Marusic (2007a) and Monty et al. (2009) that the boundary layer spectra do seem to settle to a peak with $\lambda_x \approx 2$–3δ in the outer wake region of the flow.

4.1.1 Scale separation and structure

Figure 9a–f present the energy spectra from both channels and pipes as plots at selected wall normal locations. Each plot represents a vertical slice taken from the corresponding contour maps in Fig. 8. Wall normal locations of $z^+ \approx 15, 70, 3.9\sqrt{Re_\tau}$ and $z/\delta = 0.5$ were selected as these values represent nominally the location of the energy signature of the near-wall cycle, the extreme lower limit and geometric centre of the logarithmic region and the midpoint of the channel half-height or pipe radius, respectively. Figure 9a, d show that the signature of the near-wall cycle ($\lambda_x^+ \approx 1{,}000$ energy) dominates even up to the midpoint of the logarithmic region at $Re_\tau = 1{,}000$. Energy from outer scaled modes appear only as 'shoulders' through the logarithmic region and only at $z/\delta = 0.5$ does the energetic signature of LSM appear as an energetic peak at $\lambda_x \approx 3\delta$.

For $Re_\tau = 3{,}000$, the energy distribution in the logarithmic region changes compared with the low Reynolds number cases. At the lower bound of the logarithmic region, viscous forces still dominate and a hump still appears, yet the energy plateaus across wavelengths of $1 \lesssim \lambda_x/\delta \lesssim 10$, which is indicative of LSMs. However, by the midpoint of the logarithmic region, outer-scaled motions dominate, and now a clear energetic peak exists at wavelengths of $10 \lesssim \lambda_x/\delta \lesssim 20$. This is highlighted in Fig. 9c, f. The distribution of the energy changes from 'inner' scaling to 'outer' scaling within the logarithmic region. At $z/\delta = 0.5$, an energetic peak appears at $\lambda_x = 3\delta$ with a shoulder still appearing at $10 \lesssim \lambda_x \lesssim 20$. The increased scale separation at the higher Reynolds numbers

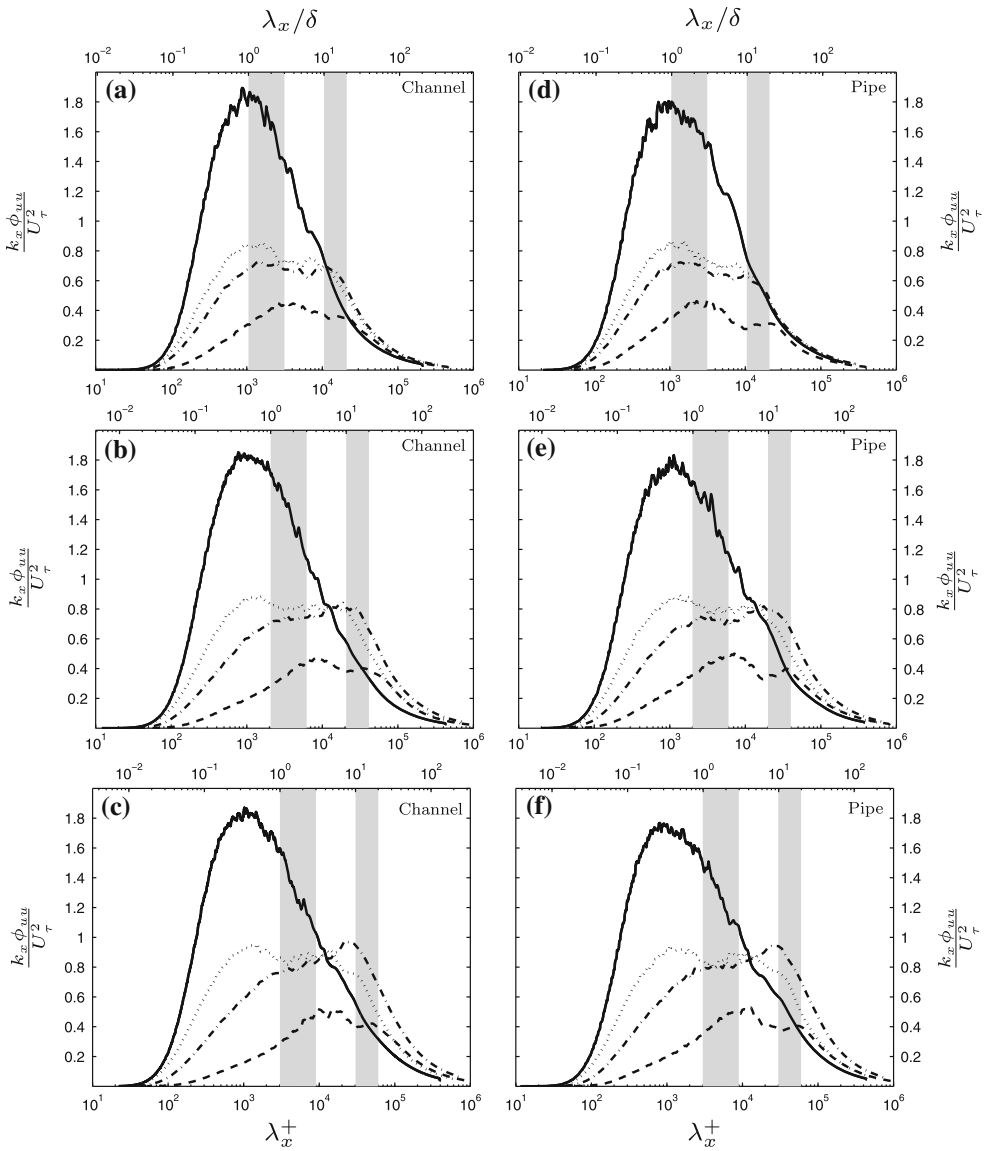

Fig. 9 *Line* plots of spectra at various wall normal locations measured using $l^+ \approx 22$. **a** Channel: $Re_\tau = 1{,}000$, **b** channel: $Re_\tau = 2{,}000$, **c** channel: $Re_\tau = 3{,}000$, **d** pipe: $Re_\tau = 1{,}000$, **e** pipe: $Re_\tau = 2{,}000$, **f** pipe: $Re_\tau = 3{,}000$. Wall normal locations: (*dash*)$z^+ \approx 15$, (*dotted lines*)$z^+ \approx 70$, (*dash* with *dotted lines*) $z^+ \approx 3.9\sqrt{Re_\tau}$ and (*broken dash*) $z^+ \approx 0.5\delta^+$. *Shaded areas* indicate LSM ($1 \leq \lambda_x/\delta \leq 3$) and VLSM ($10 \leq \lambda_x/\delta \leq 20$) wavelengths, respectively

makes identification of the outer-scaled modes much less difficult. Again, the data presented here have a constant spatial resolution; hence, the shift in energy from small to large scales with increasing wall distance/Reynolds number is not an artefact of attenuation due to sensor lengths.

4.1.2 *What causes the turbulence intensity to rise with Re_τ?*

It was shown in Sect. 3.1.2 that not only does the near-wall peak in turbulence intensity grow with Reynolds number; moreover, the turbulence intensity throughout the entire logarithmic region also rises with Reynolds number. As the streamwise turbulence intensity, $\overline{u^2}^+$ is equivalent to the area under the pre-multiplied u spectra, i.e.

$$\overline{u^2}^+ = \int_0^\infty \frac{k_x \phi_{uu}}{U_\tau{}^2} \mathrm{d}(\log k_x), \tag{4}$$

an examination of the u spectra may shed some light on the cause of the rising turbulence intensity with Reynolds number. Figure 10a shows the pre-multiplied u spectra for Reynolds numbers with matched inner wire lengths ($l^+ \approx 22$) from the channel flow at $z^+ \approx 15$. Figure 10b shows the spectra at the midpoint of the logarithmic region and Fig. 10c the streamwise turbulence intensity profiles.

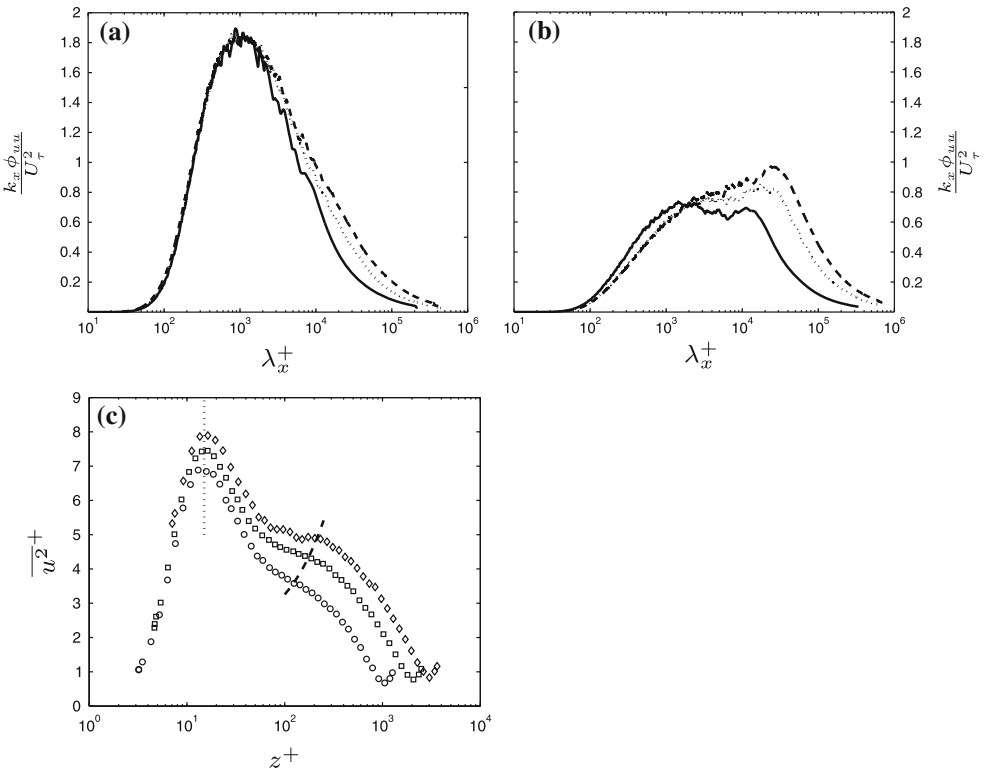

Fig. 10 Channel flow spectra at **a** $z^+ \approx 15$ and **b** $z^+ \approx 3.9\sqrt{Re_\tau}$ for $Re_\tau = 1{,}000$ (*dash*), $2,000$ (*dotted line*) and 3,000 (*broken dash*) and $l^+ \approx 22$. **c** Reproduction of Fig. 2a. *Dotted line* on plot **c** tracks near-wall peak, $z^+ = 15$, and *dashed line* tracks midpoint of logarithmic region, $z^+ \approx 3.9\sqrt{Re_\tau}$

Figure 10a reveals that the spectra collapses well in the small scales; however, with an increasing Reynolds number, there is increasing energy in the large scales. The increasing contribution at the larger scales causes the near-wall peak in turbulence intensity to rise with Reynolds number. Figure 10b shows the increasing contribution of the large scales in the centre of the logarithmic region. The spectra no longer collapse in the small scales. At $Re_\tau = 1{,}000$, the signature of the near-wall cycle is still apparent and manifests itself as a hump at the small-scale end. However, at $Re_\tau = 2{,}000$ and 3,000, the energy is dominated by large-scale motions and the hump at $\lambda_x^+ = 1,000$ is absent. Since the data here are at a constant $l^+ \approx 22$ the amount of small-scale attenuation is nominally constant. Apparent for all three Reynolds numbers is the growing contribution of the outer peak. Not only is the magnitude of the outer peak growing as expected, it is moving to increasingly large inner-scaled wavelengths, λ_x^+. However, when plotted in outer scaling, λ_x/δ, this outer peak is fixed at $10 \lesssim \lambda_x/\delta \lesssim 20$ and is the energy signature of the VLSM (see Fig. 9a–c). This increasing contribution of large-scale events in the logarithmic region at increasing Reynolds numbers causes the turbulence intensity to rise throughout the logarithmic region.

4.2 Effect of hot-wire sensor length on measured energy

An examination of the energy spectra for the data presented in Sect. 3.3 is undertaken to highlight the individual effect of l^+ and l/d on the measured u spectra and to provide some insight into the nature of attenuation observed in the turbulence intensity profiles.

4.2.1 Varying l^+ with varying Re_τ

It was shown in Sect. 3.3.1 that a varying l^+ and varying Re_τ could result in misleading behaviour of the near-wall peak turbulence intensity. This observation highlighted the competing effects of increasing Reynolds number and increasing spatial filtering (for a fixed l). Figure 11a, b are plots of the pre-multiplied u spectra at $z^+ \approx 15$ corresponding to the data plotted in Fig. 4. Here, Fig. 11a clearly demonstrates that the amount of energy attenuated in the small scales (owing to increasing inner scaled wire length) is much greater than the increasing contribution of the largescale energy for increasing Reynolds number when $22 \leq l^+ \leq 72$, causing the attendant reduction in $\overline{u^2}^+|_m$. Figure 11b demonstrates that when the wire length

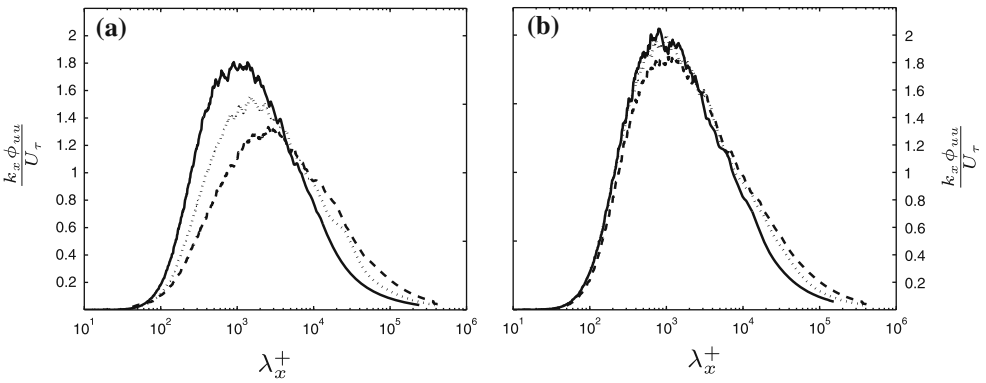

Fig. 11 Channel flow u spectra at $z^+ \approx 15$ for data presented in Fig. 4. Plot **a**: (*dash*) $Re_\tau = 1,000\, l^+ = 22$, (*dottedline*) $Re_\tau = 2,000\, l^+ = 49$ and (*broken dash*) $Re_\tau = 3{,}000\ l^+ = 72$. Plot **b**: (*solidlines*) $Re_\tau = 1,000\, l^+ = 7$, (*dottedline*) $Re_\tau = 2,000\, l^+ = 14$ and (*broken dash*) $Re_\tau = 3{,}000\ l^+ = 21$

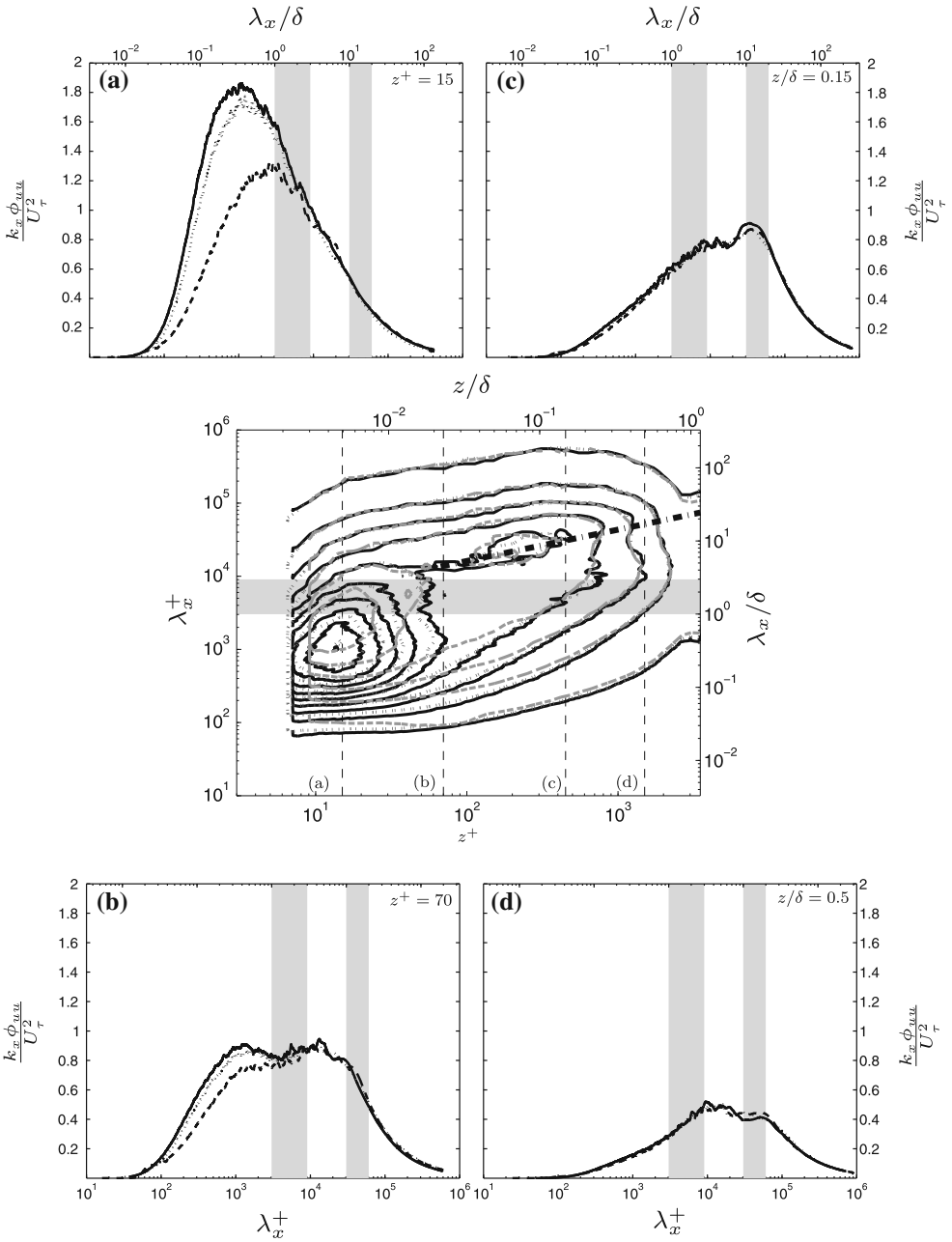

Fig. 12 Contours of channel flow u spectra for $Re_\tau = 3{,}000$ at varying inner-scaled wire lengths. (*dash*) $l^+ = 22$, (*dottedline*) $l^+ = 33$ and (*broken dash*) $l^+ = 72$. Contour levels are from $k_x\phi_{uu}/U_\tau{}^2 = 0.1$ to 1.7 in increments of 0.2. *Shaded area* indicates LSM ($1 \le \lambda_x/\delta \le 3$) and the *heavy dot-dashed line* represents VLSM growth according to Eq. 3. Slices taken as indicated at wall normal locations: **a** $z^+ \approx 15$, **b** $z^+ \approx 70$, **c** $z/\delta \approx 0.15$ and **d** $z/\delta \approx 0.5$

is small ($7 \leq l^+ \leq 22$), the contribution of the large-scale energy for increasing Reynolds number approximately balances the amount of small-scale energy being attenuated, hence the constant value of $\overline{u^2}^+|_m$. This helps to explain previous reports that $\overline{u^2}^+|_m$ does not grow with Reynolds number (for example, Mochizuki and Nieuwstadt 1996) and further reinforces that the recommendation of Ligrani and Bradshaw (1987) that $l^+ \lesssim 20$ should be reconsidered given the amount of small-scale attenuation observed here for $7 \leq l^+ \leq 22$.

4.2.2 Spatial resolution: varying l^+ for $Re_\tau = 3{,}000$ and $l/d \gtrsim 200$

Section 3.3.2 dealt with the first- and second-order moments at $Re_\tau = 3{,}000$ with various wire lengths ($l^+ = 21$, 35 and 72). Figure 12 plots contours of the corresponding pre-multiplied u energy spectra as a function of streamwise wavelength and wall normal position. Plots 12a–d are slices taken at wall normal locations of $z^+ = 15$, 70, $0.15\delta^+$ and $0.5\delta^+$.

At $z^+ = 15$, the increasing sensor size is causing an attenuation of the measured energy in the small scales. The spectra collapse at the larger wavelengths for all wire sizes investigated here. Therefore, not only is the maximum recorded energy decreasing with increasing l^+, the peak energy is moving to larger λ_x^+. The missing small-scale energy is responsible for the reduction in measured turbulence intensity at the near-wall peak as shown in Fig. 5b. At $z^+ = 70$, the energy signature of the near-wall cycle is still present; however, there is a clear contribution from large-scale events which manifests as a secondary hump, as discussed in Sect. 4.1.1. Here, the attenuation of the near-wall cycle energy is still apparent although not as pronounced and, again, the spectra collapse LSM and VLSM wavelengths. This collapse indicates that the measured energy is well resolved for $z/\delta \gtrsim 0.15$ even with the largest wire. Indeed, the turbulence intensity profiles in Fig. 5b ($Re_\tau = 3{,}000$ and $21 < l^+ < 72$) exhibit very good similarity for $z/\delta \gtrsim 0.15$.

The amount of attenuation owing to increasing l^+ appears to be scale dependent (both in the streamwise and in spanwise directions) and hence dependent on the wall normal location of the probe. This is due to the fact that the flow is highly anisotropic and that the dominant ratio of streamwise-to-spanwise wavelengths (λ_x/λ_y) is changing with wall distance, as shown in the two-dimensional u spectra from channel flow DNS (see for example, del Álamo et al. 2004; Jiménez and Hoyas 2008). Since the hot-wire sensor may be considered a filter of fixed spanwise wavelength, λ_y, the amount of energy attenuated at a given streamwise wavelength changes with wall distance. Near the wall, λ_x/λ_y approaches 10, the small scales dominate and attenuation is greatest because l^+ is large relative to the dominant λ_y^+. Moving away from the wall, λ_x/λ_y is still large, but l^+ becomes small relative to the dominant λ_y^+. Therefore, the wall distance at which small-scale attenuation is still appreciable depends on the size of the wire. This is clearly demonstrated in Fig. 12 by the improving convergence of the $k_x\phi_{uu}/U_\tau^2$ contours with increasing wall distance and streamwise wavelength.

4.2.3 Length-to-diameter ratio: fixed $l^+ \approx 22$ for $Re_\tau = 3{,}000$ and varying l/d

In Sect. 3.3.3, mean statistics for pipe flow at $Re_\tau = 3{,}000$ and $l^+ \approx 22$ for $l/d = 77$, 146, 244 and 365 were presented. It was revealed that an insufficient hot-wire length-to-diameter ratio causes a reduction in magnitude of the measured broadband turbulence intensity profile across the entire turbulent flow. For sufficient l/d (i.e. $\gtrsim 200$), there was no appreciable difference in the measured turbulence intensity. Here, the corresponding pre-multiplied u spectra is presented in an identical manner to Fig. 12, except here each contour represents a different l/d for a fixed $l^+ = 22$. For consistency, slices are taken at the same wall normal locations as Sect. 4.2.2.

Figure 12 showed that attenuation of measured energy due to spatial resolution is likely a complex function of wire length, wall distance and Reynolds number due to the anisotropic nature of the flow. This was indicated by the degree of collapse of the spectra contours with a particular wall distance and wavelength for a value of l^+. In contrast, Fig. 13 shows that the attenuation caused by insufficient l/d is fundamentally different in nature. This is reflected by the lack of convergence of the $k_x\phi_{uu}/U_\tau^2$ contours with increasing wall distance and streamwise wavelength. Note that in Fig. 13a, the energy at $z^+ = 15$ only exhibits a reduction in magnitude and still peaks at $\lambda_x^+ \approx 1{,}000$, whereas a shift in the peak energy with increasing l^+ was shown in Fig. 12. When moving away from the wall (Fig. 13b–d), it becomes clear that l/d is not confined to the near-wall region and that an insufficient l/d affects almost the entire turbulent flow. For $l/d = 77$ and 146, the missing energy is not confined to small scales near the wall, but rather attenuation is observed for a very broad range of streamwise wavelengths extending into the logarithmic and outer regions with missing energy still apparent beyond wall distances of $z/\delta = 0.5$. For $l/d = 244$ and 365, however, the spectra collapse well in both wall distance and streamwise wavelength, suggesting that the criterion recommended by Ligrani and Bradshaw (1987) of $l/d \geq 200$ is sufficient for the flow regime reported in this paper.

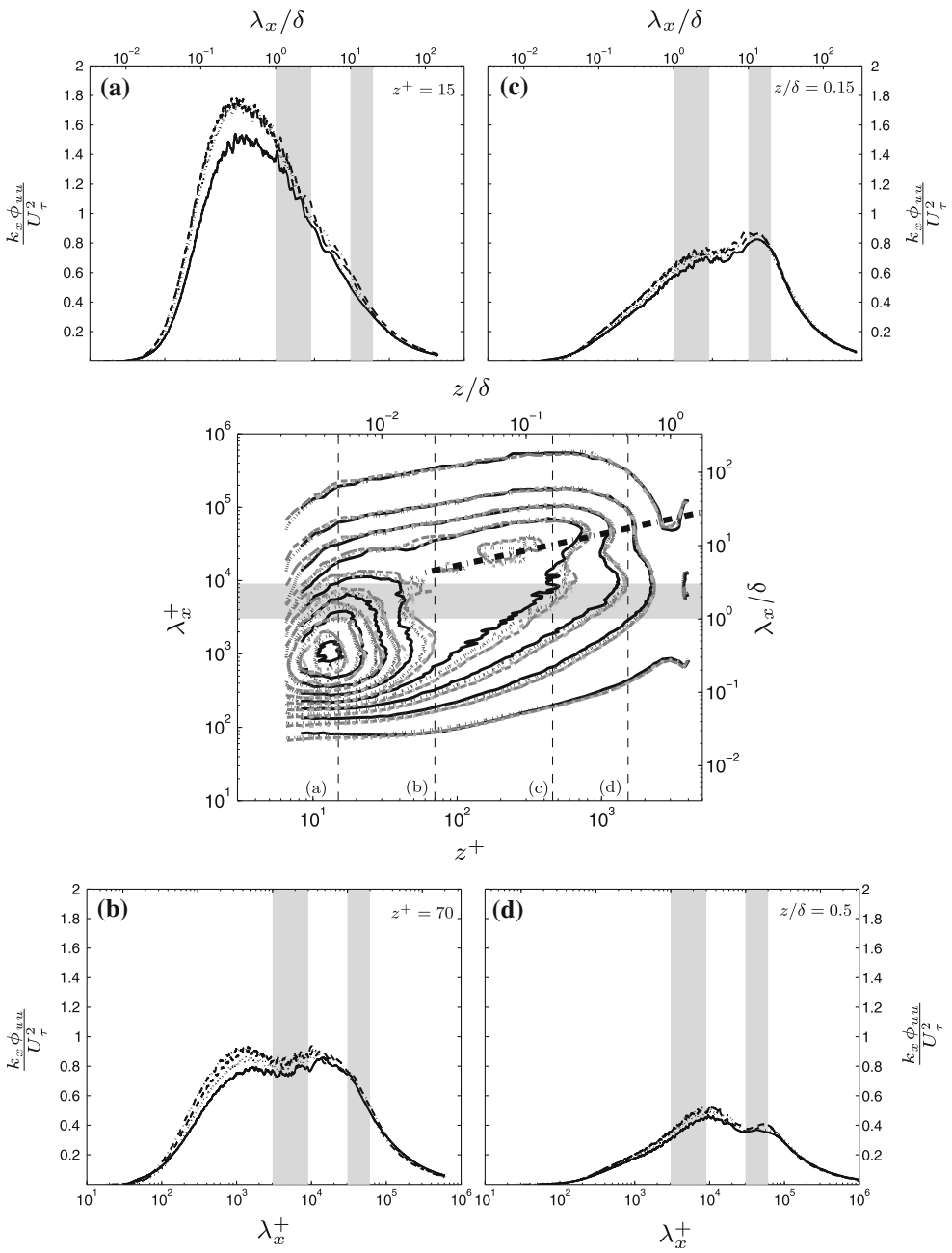

Fig. 13 Contours of pipe flow u spectra for $Re_\tau = 3{,}000$ at matched inner-scaled wire length of $l^+ \approx 22$ for varying l/d. (*dash*) $l/d = 77$, (*dottedline*) $l/d = 146$, (*dashedline*) $l/d = 244$ and (*broken dash*) $l/d = 365$. Contour levels are from $k_x\phi_{uu}/U_\tau{}^2 = 0.1$ to 1.7 in increments of 0.2. *Shaded area* indicates LSM ($1 \leq \lambda_x/\delta \leq 3$) and the *heavy dot-dashed line* represents VLSM growth according to Eq. 3. Slices taken as indicated at wall normal locations: **a** $z^+ \approx 15$, **b** $z^+ \approx 70$, **c** $z/\delta \approx 0.15$ and **d** $z/\delta \approx 0.5$

Whilst it is well established that an insufficient hot-wire aspect ratio will lead to attenuation caused by heat loss due to end conduction, the spectral information presented in Figs. 12 and 13 show that an attenuation of the measured turbulence intensity due to l^+ and l/d is brought about in different ways. Importantly, the amount of attenuation and wavelengths that are affected by spatial filtering is heavily dependent on the wall distance (and therefore local Reynolds number) due to the anisotropy of the flow; however, the attenuation due to l/d is much less sensitive to wall distance and affects almost the entire range of streamwise lengthscales. This would suggest that insufficient l/d is akin to a damper that affects a hot-wire's ability to respond to velocity fluctuations of any length scale, whereas l^+ effects are akin to a spanwise spatial filter that affects the hot-wire's ability to respond to small-scale velocity fluctuations. The relationship between l^+, λ_y and λ_x is not well defined and would require velocity measurements in both the streamwise and spanwise directions. Further complications arise because for a changing l^+ and l/d, Re_w must also be changing which will most likely be accompanied by a change in stub geometry. A full parametric study of all these parameters would be almost intractable due to the sheer number of experiments that would be required. This section therefore further reinforces that hot-wire sensor parameters need to be carefully controlled.

5 Conclusions

This paper presents new experimental measurements of velocity statistics and spectra in fully developed turbulent channel and pipe flows for Reynolds numbers $1{,}000 \leq Re_\tau \leq 3{,}000$. The channel flow and pipe flow facilities have a nominally equivalent outer length scale and careful matching of the inner-scaled wire length at various Reynolds numbers allows for direct comparison of the two flows. Effects of hot-wire spatial resolution and hot-wire length-to-diameter ratio were also examined. The following is a summary of the main findings.

1. *The inner-scaled turbulence intensity, $\overline{u^2}^+|_m$, rises with Reynolds number*. By matching l^+ and using $l/d \gtrsim 200$, the effects of spatial resolution and stub-convection on the probes are isolated from the competing effect of the Reynolds number. It can be seen that the recorded maximum value of $\overline{u^2}^+|_m$, located at $z^+ \approx 15$, rises with Reynolds number in both channel and pipe flows for $1{,}000 < Re_\tau < 3{,}000$, which is in contrast to recent results by Hultmark et al. (2010) for pipe flows. We show that the increase in $\overline{u^2}^+|_m$ is caused by the increasing presence of large-scale energy in the near-wall region. The Reynolds number dependence of $\overline{u^2}^+|_m$ is consistent for channels, pipe and boundary layers, however, it must be noted that Buschmann and Gad-el-Hak (2010) report that the observed trends of the cross stream components of the Reynolds normal stresses, $\overline{v^2}^+$ and $\overline{w^2}^+$ are different for internal and external flows.
2. *Channel and pipe flows exhibit similar velocity statistics and spectra*. It was revealed that channel and pipe flows are very similar both statistically and spectrally within the near-wall and logarithmic regions. In the outer region, the pipe flow exhibits a stronger wake than the channel flow as evidenced by the larger deviation from the logarithmic law of the wall. However, the difference in wake strength between the two flows is not reflected in the turbulence intensity or the u spectra, which are very similar over the entire layer. These findings agree well with Monty et al. (2009) and the measurements with matched hot-wire length confirm that the increasing contributions of LSM and VLSM events with increasing Reynolds number are not an artefact of small-scale energy attenuation caused by spatial resolution issues.
3. *The need for higher Reynolds number, constant spatial resolution data from turbulent channel and pipe flows*. In order to clearly separate the small-scale contribution dominated by the near-wall cycle ($\lambda_x^+ = 1{,}000$ energy) and the large-scale contributions from the LSM events ($\lambda_x = 1 - 3\delta$) and VLSM events ($\lambda_x = 12 - 14\delta$), higher Reynolds number channel and pipe flow data will be required. The Reynolds numbers in this study only achieve a good separation of the small scales and VLSM events, but not between the small scales and the LSM events. Furthermore, an extended overlap region is only achieved for the highest Reynolds number. This is important not only for the determination of the functional form of the mean velocity distribution but also because coherent turbulent structures presiding in the overlap region have been shown to affect near-wall turbulence, which has important implications for flow control studies.
4. *Lack of comparison between higher Reynolds number DNS and experiments*. To date, a lack of direct comparison between experiments and higher Reynolds number DNS data exists (Monty and Chong 2009 notwithstanding). With high Reynolds numbers DNS studies now approaching those of typical laboratory scale measurements, the lack of comparison between DNS and experiments is, in large part, due to the lack of well-resolved experimental data, as Jiménez (2003) clearly stated. Therefore, the new experiments presented in this paper appear timely and may provide a database of well resolved measurements suitable for comparison to DNS studies.
5. *Make l^+ as small as possible and keep constant if possible*. When making hot-wire measurements of velocity, careful consideration should be given to this parameter. For internal flows, a fixed physical sensor length (l) will lead to an increasing inner-scaled wire length (l^+) with increasing Reynolds number. As l^+ increases, the measured velocity fluctuations become increasingly under resolved because the sensor acts akin to a spatial filter. Section 4.2.2 reveals that attenuation due to l^+ effects is scale dependent and that the longer the wire, the less small-scale energy the sensor can resolve. The missing small-scale energy provides a good explanation as to the observation that the near-wall measured turbulence intensity is increasingly attenuated with increasing l^+. Further, it was shown that if l^+ is allowed to vary simultaneously with Reynolds number, the near-wall peak in the turbulence intensity can be observed to diminish with increasing Re_τ or conversely to remain constant with increasing Re_τ (depending on the range of l^+ values). Therefore, when drawing conclusions regarding flow physics or when making comparisons across facilities or Reynolds numbers, it is preferable to remove the spatial resolution effects. The above conclusion also applies to l/η where η is the Kolmogorov length scale as discussed by Hutchins et al. (2009).

6. *$l/d \geq 200$ appears necessary and sufficient for pure platinum hot-wires and conditions studied here*. Insufficient l/d was shown to cause significant attenuation of the measured u spectra and hence turbulence intensity. The attenuation from insufficient l/d was different in nature to that of an l^+ effect. The energy attenuation seemed to not only occur in the small scales, but for small l/d, there is a appreciable attenuation of large-scale energy. The missing energy due to insufficient l/d did not appear confined to the near-wall region and logarithmic regions. It was shown that the critical value of l/d required to resolve the most energetic portion of the flow is very close to $l/d = 200$ for pure platinum hot-wires operating in nominally atmospheric conditions and typical velocities. Further work is required in order to understand how different wire materials may effect the critical hot-wire length-to-diameter ratio.

This study only attempts to control for two parameters, namely l^+ and l/d, and there is evidence to suggest that measured turbulence is a complex function of various other parameters including the hot-wire Reynolds number and wire materials. A full investigation of all sensor parameters would be practically prohibitive due to limited availability of wire diameters and the requirement that sensor sizes would have to continually diminish with increasing Reynolds number for a given facility. While this paper only deals with u statistics and spectra, it would appear to be of some value to make measurements of the cross-stream components of velocity in a manner similar to that described in this paper (i.e. matched anemometer parameters) to confirm the trends reported in the literature.

Acknowledgments The authors are grateful for the financial support of the Australian Research Council through grants FF0668703, DP0984577 and DP0663499.

References

Balakumar BJ, Adrian RJ (2007) Large and very-large-scale motions in channel and boundary-layer flows. Philos Trans R Soc A 365:665–681

Bruun HH (1995) Hot-Wire anemometry: principles and signal analysis, 1st edn. Oxford University Press, New York

Buschmann MH, Gad-el-Hak M (2009) Evidence of nonlogarithmic behaviour of turbulent channel and pipe flow. AIAA J 47(3):535–541

Buschmann MH, Gad-el-Hak M (2010) Normal and cross-flow Reynolds stresses: difference between confined and semi-confined flows. Exp Fluids 49(1):213–223

Chin CC, Hutchins N, Ooi ASH, Marusic I (2009) Use of DNS data to investigate spatial resolution issues in measurements of wall bounded turbulence. Meas Sci Technol 20:115401

Chung D, McKeon BJ (2010) Large-eddy simulation of large-scale flow structures in long channel flow. J Fluid Mech 661:341–364

Comte-Bellot G (1965) Ecoulement turbulent entre deux parois paralleles. Technical Report 419, Publications Scientifiques et Techniques du Ministere de l'Air

DeGraaff DB, Eaton JK (2000) Reynolds-number scaling of the flat-plate turbulent boundary layer. J Fluid Mech 422:319–346

del Álamo J, Jiménez J (2009) Estimation of turbulent convection velocities and corrections to Taylor's approximation. J Fluid Mech 640:5–26

del Álamo J, Jiménez J, Zandonade P, Moser RD (2004) Scaling of energy spectra in turbulent channels. J Fluid Mech 500:135–144

Dennis DJC, Nickels TB (2008) On the limitations of Taylor's hypothesis in constructing long structures in a turbulent boundary layer. J Fluid Mech 614:197–206

Durst F, Jovanovic J, Sender J (1995) LDA measurements in the near-wall region of a turbulent pipe flow. J Fluids Mech 295:305–335

Eggels JGM, Unger F, Weiss MH, Westerweel J, Adrian RJ, Friedrich R, Nieuwstadt FTM (1994) Fully developed turbulent pipe flow: a comparison between direct numerical simulation and experiment. J Fluid Mech 268:175–209

Fernholz HH, Finley PJ (1996) The incompressible zero-pressure-gradient turbulent boundary layer: an assessment of the data. Prog Aerosp Sci 32:245–311

Guala M, Hommema SE, Adrian RJ (2006) Large-scale and very-large-scale motions in turbulent pipe flow. J Fluid Mech 554:521–542

Hoyas S, Jiménez J (2006) Scaling of velocity fluctuations in turbulent channel flows up to $Re_\tau = 2003$. Phys Fluids 18:011702

Hoyas S, Jiménez J (2008) Reynolds number effects on the Reynolds-stress budgets in turbulent channels. Phys Fluids 20:101511

Hultmark M, Bailey SCC, Smits AJ (2010) Scaling of near-wall turbulence intensity. J Fluid Mech 649:103–113

Hutchins N, Marusic I (2007a) Evidence of very long meandering features in the logarithmic region of turbulent boundary layers. J Fluid Mech 579:1–28

Hutchins N, Marusic I (2007b) Large-scale influences in near-wall turbulence. Philos Trans R Soc A 365:647–664

Hutchins N, Nickels T, Marusic I, Chong M (2009) Hot-wire spatial resolution issues in wall-bounded turbulence. J Fluid Mech 635:103–136

Iwamoto K, Fukagata K, Kasagi N, Suzuki Y (2004) DNS of turbulent channel flow at $Re_\tau = 1160$ and evaluation of feedback control at practical reynolds numbers. In: Proceedings of the fifth symposium smart control of turbulence, 29 Feb–2 March

Iwamoto K, Kasagi N, Suzuki Y (2005) Direct numerical simulation of turbulence channel flow at $Re_\tau = 2320$. In: Proceedings of the sixth symposium smart control of turbulence, Tokyo

Jiménez J (2003) Computing high-reynolds number turbulence: will simulations ever replace experiments? J Turbul 4(22). doi: 10.1088/1456-5248/4/1/022

Jiménez J, Hoyas S (2008) Turbulent fluctuations above the buffer layer of wall-bounded turbulence. J Fluid Mech 611:215–236

Johansson AV, Alfredsson PH (1982) On the structure of turbulent channel flow. J Fluid Mech 122:295–314

Johansson AV, Alfredsson PH (1983) Effects of imperfect spatial resolution on measurements of wall-bounded turbulent shear flows. J Fluid Mech 137:409–421

Jorgensen FE (1996) The computer-controlled constant-temperature anemometer. Aspects of set-up, probe calibration, data acquisition and data conversion. Meas Sci Technol 7:1378–1387

Kim J, Moin P, Moser R (1987) Turbulence statistics in fully developed channel flow at a low Reynolds number. J Fluid Mech 177:133–166

Kim KC, Adrian RJ (1999) Very large-scale motion in the outer layer. Phys Fluids 11(2):417–422

Kline S, McClintock FA (1953) Describing uncertainties in single sample experiments. Mech Eng 75(1):38

Kline S, Reynolds W, Shrub F, Rundstadler P (1967) The structure of turbulent boundary layers. J Fluid Mech 30:741–773

Laufer J (1950) Investigation of turbulent flow in a two-dimensional channel. Technical Report 1053, National Advisory Committee for Aeronautics

Laufer J (1954) The structure of turbulence in fully developed pipe flow. Technical Report 1174, National Advisory Committee for Aeronautics

Lawn CJ (1971) The determination of the rate of dissipation in turbulent pipe flow. J Fluid Mech 48:477–505

Li JD, McKeon BJ, Jiang W, Morrison JF, Smits AJ (2004) The response of hot wires in high Reynolds-number turbulent pipe flow. Meas Sci Technol 15:789–798

Ligrani P, Bradshaw P (1987) Spatial resolution and measurement of turbulence in the viscous sublayer using subminiature hot-wire probes. Exp Fluids 5:407–417

Marusic I, Kunkel GJ (2003) Streamwise turbulence intensity formulation for flat plat-plate boundary layers. Phys Fluids 15(8):2461–2464

Marusic I, Uddin AKM, Perry AE (1997) Similarity laws for the streamwise turbulence intensity in zero-pressure-gradient turbulent boundary layers. Phys Fluids 9(12):3718–3726

Marusic I, McKeon BJ, Monkewitz PA, Nagib HM, Smits AJ, Sreenivasan KR (2010) Wall-bounded turbulent flows at high Reynolds numbers: recent advances and key issues. Phys Fluids 22:065103

Mathis R, Hutchins N, Marusic I (2009a) Large-scale amplitude modulation of the small-scale structures in turbulent boundary layers. J Fluid Mech 628:311–337

Mathis R, Monty J, Hutchins N, Marusic I (2009b) Comparison of large-scale amplitude modulation in boundary layers, pipes and channel flows. Phys Fluids 21:111703

McKeon BJ, Li J, Jiang W, Morrison JF, Smits AJ (2004) Further observations on the mean velocity distribution in fully developed pipe flow. J Fluid Mech 501:135–147

Metzger M, Klewicki J (2001) A comparative study of near-wall turbulence in high and low Reynolds number boundary layers. Phys Fluids 13(3):692–701

Mochizuki S, Nieuwstadt FTM (1996) Reynolds-number-dependence of the maximum in the streamwise velocity fluctuations in wall turbulence. Exp Fluids 21:218–226

Moin P (2009) Revisiting Taylor's hypothesis. Journal of Fluid Mechanics 640:1–4

Monty JP (2005) Developments in smooth wall turbulent duct flows. Ph.D. thesis, The University of Melbourne

Monty JP, Chong MS (2009) Turbulent channel flow: comparison of streamwise velocity data from experiments and direct numerical simulation. J Fluid Mech 633:461–474

Monty JP, Stewart JA, Williams RC, Chong MS (2007) Large-scale features in turbulent pipe and channel flows. J Fluid Mech 589:147–156

Monty JP, Hutchins N, Ng H, Marusic I, Chong MS (2009) A comparison of turbulent pipe, channel and boundary layer flows. J Fluid Mech 632:431–442

Morrison J, McKeon B, Jiang W, Smits A (2004) Scaling of the streamwise velocity component in turbulent pipe flow. J Fluid Mech 508:99–131

Morrison WRB, Kronauer RE (1969) Structural similarity for fully developed turbulence on smooth tubes. J Fluid Mech 39:117–141

Nagib HM, Chauhan K (2008) Variations of von Kármán coefficient in canonical flows. Phys Fluids 20:101518

Niederschulte MA, Adrian RJ, Hanratty TJ (1990) Measurements of turbulent flow in a channel at low Reynolds numbers. Exp Fluids 9:222–230

Perry AE, Abell C (1975) Scaling laws for pipe-flow turbulence. J Fluid Mech 67:257–271

Perry AE, Henbest S, Chong MS (1986) A theoretical and experimental study of wall turbulence. J Fluid Mech 165:163–199

Perry AE, Hafez S, Chong MS (2001) A possible reinterpretation of the princeton superpipe data. J Fluid Mech 439:395–401

Taylor GI (1938) The spectrum of turbulence. Proc R Soc Lond A 164:476–490

den Toonder JMJ, Nieuwstadt FTM (1997) Reynolds number effects in a turbulent pipe flow for low to moderate Re. Phys Fluids 9(11):3398–3409

Wei T, Willmarth WW (1989) Reynolds-number effects on the structure of a turbulent channel flow. J Fluid Mech 204:57–95

Wu X, Moin P (2008) A direct numerical simulation study on the mean velocity characteristics in turbulent pipe flow. J Fluid Mech 608:81–112

Yavuzkurt S (1984) A guide to uncertainty analysis of hot-wire data. J Fluids Eng 106:181–186

Zagarola M, Smits A (1998) Mean flow scaling in turbulent pipe flow. J Fluid Mech 373:33–79

Zanoun ES, Durst F, Nagib H (2003) Evaluating the law of the wall in two-dimensional fully developed turbulent channel flows. Phys Fluids 15(10):3079–3089